Faculty of Health Science
Department of Pharmacy
Drug Transport and Delivery Research Group

Chitosan Lecithin Nanoparticles with New Chemical Entity

Nanotoxicity Evaluation

—

Lloyd Mbugua Kangu
Master thesis in Pharmacy, May 2016

SUPERVISORS
Professor Nataša Škalko-Basnet
Doctor Gry Stensrud

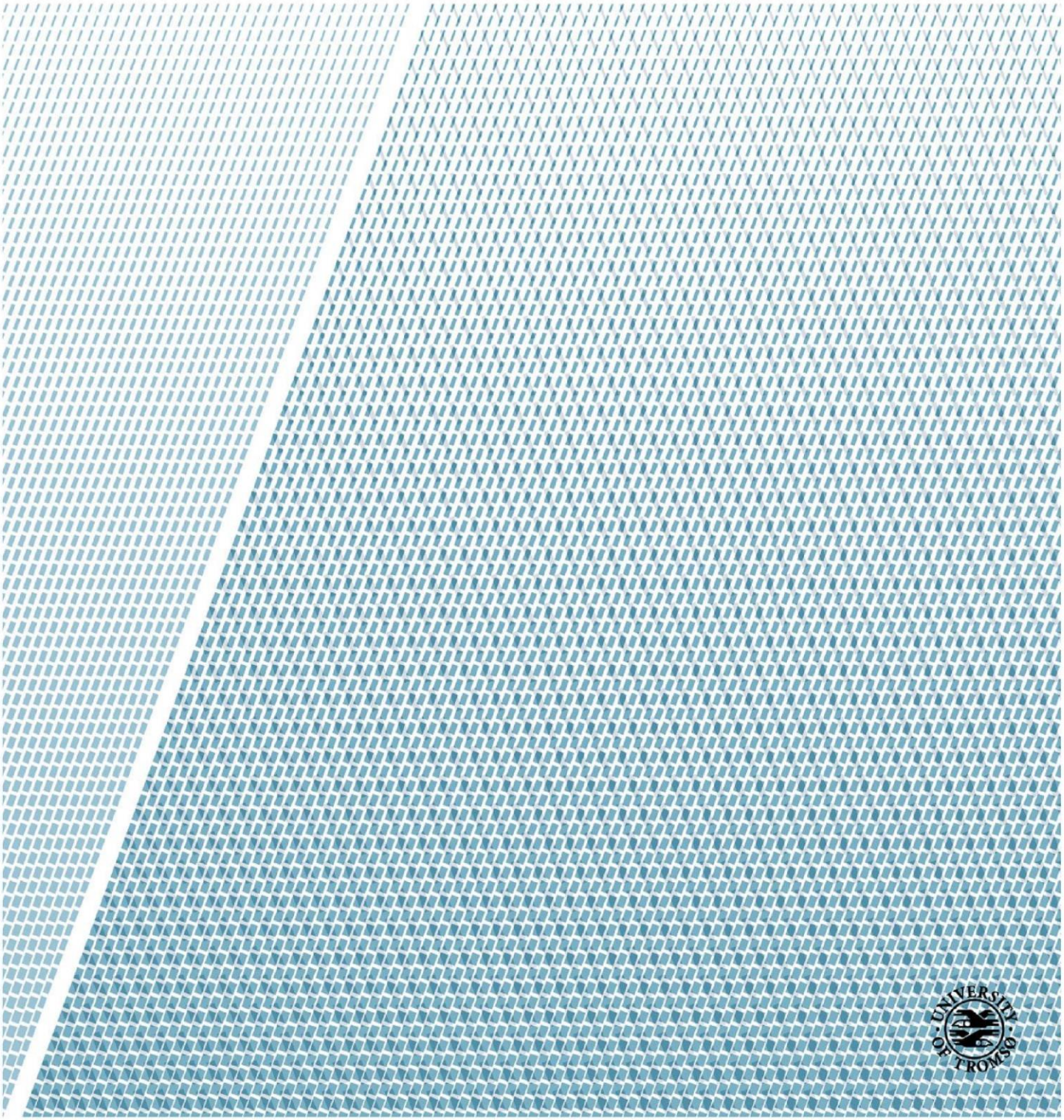

MATER THESIS FOR THE DEGREE MASTER OF PHARMACY

CHITOSAN LECITHIN NANOPARTICLES WITH NEW CHEMICAL ENTITY

BY

LLOYD MBUGUA KANGU

MAY 2016

SUPERVISORS

Professor Nataša Škalko-Basnet
Head of Drug Transport and Delivery Group,
Institute of Pharmacy,
The University of Tromsø

and

Gry Stensrud
Vice President Technical Development and Operations,
Photocure ASA

Drug Transport and Delivery Research Group

Department of Pharmacy

Faculty of Health Sciences

The University of Tromsø – The Arctic University of Norway

In loving memory of my cũcũ, Sabina Nduta Njuguna (1943 – 2015)

Acknowledgements

The following work in this thesis was carried out at the Drug Transport and Delivery Research Group, Department of Pharmacy, University of Tromsø The Arctic University of Norway, Norway from September 2015 to May 2016.

I would first like to thank my thesis supervisor Professor Nataša Škalko-Basnet of the Department of Pharmacy at University of Tromsø. I extend to you my deepest and most sincere gratitude for your encouragement, guidance, patience, and support throughout the entirety of the project, but especially after the loss of my grandmother. Words cannot express my sincere appreciation for this. Truly. I am certain that my completion of the thesis is fully honoured to your affection for students. The door to Professor Škalko-Basnet's office was always open whenever I had a question about the research or writing, and if not she swiftly responded to any queries by e-mail. Thanks you for sharing a seemingly infinite, and at minimum profuse amount of knowledge with me. Thank you.

I would also like to thank my second supervisor Doctor Gry Stensrud at Photocure ASA for our collaboration. I wish to extend my gratitude both to Doctor Stensrud and Photocure ASA for letting me be privileged enough to work on this assignment aboard you.

Thanks to Chitinor AS for providing the chitosan used during this project.

I would further like to thank the Drug Transport and Delivery Research Group, for welcoming me with open arms, and for having a very friendly and quite stimulating research environment. Special thanks to Associate Professor Ann Mari Holsæter and Massimiliano Di Cagno, Ph.D. students Sveinung G. Ingebrigtsen, Iren Y. Wu, and Selenia Ternullo for sacrificing your valuable time in order to help me in the laboratory and/or answering my questions.

Thanks to Cristiane de Albuquerque Cavalcanti Jacobsen for your help with technical matters, and especially for teaching me about the HaCaT cells and the MTT assay. I would be doing you disfavour if I did not mention how contagious your cheerfulness is, in addition to this you were always supportive when I was confronted with difficulties in the laboratory.

I would like to thank my fellow master students in our research group: Awfa Alshamkawy, and both Margherita Falavigna and Camilla Duedahl Hendé and for the limited time they have spent with us. I wish you all the best in your future endeavours.

My continued thankfulness goes to my fellow students at the Department of Pharmacy as well as other students at the University of Tromsø for making my student years quite memorable, and initiating what I believe is going to be life-long friendships. Thank you Damir Dugalic, Edmund T. F. Assignon, Kristian M. Sørensen, Abel Teckle, Nikolai Ciric, Peter Moen, and Stine Andersen.

Finally, I must express my very profound gratitude to my family and my friends for providing me with unfailing support and continuous encouragement throughout my years of study and through the process of researching and writing this thesis. A special thanks to these friends: Bjørn Carlos Aranda Velasquez, Rikke de Lange, Stine Antonsen, Morten Tranung, Karoline Mauland Frantzen, Einar Dagsland Nerheim, Simen Østerhus Ledaal, and Irja Kjærvik. This accomplishment would not have been possible without them. Thank you.

- *Lloyd Mbugua Kangu, May 2016*

Table of Contents

List of Figures

List of Tables

List of Abbreviations

5-ALA /ALA	5 aminolevulinic acid
AHL	Acyl homoserine lactone
AI-2	Autoinducer-2
ALAS	ALA synthase
AMP	Antimicrobial peptides
APDT	Antimicrobial photodynamic therapy
CCS	Concentrated cell solution
CL	Chitosan/Lecithin
CPO	Coproporhyrinogen oxidase
EE	Entrapment efficiency
ELISA	Enzyme-linked immunosorbent assay
FBS	Fetal bovine serum
HaCaT cell	Immortal keratinocyte cell
HAL	Hexaminolevulinate
HPLC	High performance liquid chromatography
MAL	Methylaminolevulinate
MEM	Minimum essential medium
MTT	3-[4,5-dimethylthiazol-2-yl]-2,5-diphenyltetrazoliumbromide
OD	Optical density
NP	Nanoparticles
NCE	New chemical entity
PBS	Phosphate-buffered saline
PCA	Polycyanoacrylate
PDT	Photodynamic therapy
PDTA	Photodynamic therapy agent
PGA	Polyglycolic acid
PI	Polydispersity index
PLA	Polylactic acid
PLGA	Poly lactic-co-glycolic acid
PLP	Pyridoxal-5-phosphate
PpIX	Protoporphyrin IX

PPO	Protoporphyrinogen
PROTO X	Protoporphyrinogen III
PS	Photosensitizer
QS	Quorum sensing
ROS	Reactive oxygen species
RPMI	Roswell Park Memorial Institute medium
RR	Relative Recovery
SD	Standard deviation
SC	Stratum corneum
ZP	Zeta potential

Abstract

Chronic skin wounds are an exponentially increasing problem on a world basis, and are often hard to treat due to bacterial biofilm formation and resistance to different antibiotic treatments. Antimicrobial photodynamic therapy (aDPT) shows promise in resolving this issue, but clinical based treatments have yet to be established although photodynamic therapy is used for other conditions.

A new chemical entity (NCE) encapsulated in chitosan/lecithin nanoparticles as well as NCE as a free drug was evaluated for potential cytotoxic effects by an *in vitro* MTT assay performed on HaCaT cells. The nanoparticles were varying in mean size (173.9±69.2 to 486.3±197.9) and zeta potential (16.5±1.67 to 66.3±1.15); depending on the chitosan/lecithin ratio, and the entrapment was between 42.1±0.3 to 84.4±0.2 %. To evaluate the cytotoxic effect different solutions of free NCE (50 to 500 mg/mL) and NCE in the nanoparticles (103.1 to 824.8 μg/mL) were tested. The results found non-significant decreases in cell viability for the lower concentrations, as well as significant increases in cell viability higher concentrations. Although NCE showed promising results with little to no toxicity in both formulations, further testing needs to be conducted before a final toxicity assessment can be made.

Keywords: MTT assay; HaCaT cells; photodynamic therapy; chronic wounds; drug delivery system; nanoparticles

Sammendrag

Kroniske hudsår er et økende problem på verdens basis, og er ofte vanskelige å behandle grunnet bakterienes biofilmdannelse og dermed økt resistens mot ulike antibiotika behandlingsregimer. Antimikrobiell fotodynamisk terapi har vist å være en lovende legemiddelkandidat mot antibiotikaresistens, men det fins foreløpig ingen etablerte kliniske behandlinger slik i de andre anvendte felte av fotodynamisk terapi.

En ny kjemisk substans (NCE) ble inkorporert i kitosan/lecitin nanopartikler og løst i et medium for å utforske de potensielle cytotoksisk effekten som kan bli utøvd. Dette ble gjort via et *in vitro* MTT forsøk på HaCaT celler. Nanopartiklene varierte i gjennomsnittsstørrelse (173.9±69.2 to 486.3±197.9) og zetapotensial (16.5±1.67 to 66.3±1.15) avhengig av kitosan/lecitin forholdet. Inkorporeringen av NCE var på 42.9 to 84.4%. Resultatene viste ikke-signifikante reduksjoner av celleoverlevelse for de lavere NCE konsentrasjonene, mens det samtidig også viste signifikante økninger i celleoverlevelse ved de høyere konsentrasjonene. Til tross for at NCE viste lovende resultater i henhold til celleoverlevelse med lite til ingen toksisitet, må videre testing utføres før man kan komme med et konklusivt utsagn vedrørende toksisiteten.

Nøkkelord: MTT assay; HaCaT celler; fotodynamisk terapi; kroniske hudsår; drug delivery systemer; nanopartikler

1 Introduction

1.1 Wound care costs to society

In the US alone chronic wounds affect an flabbergasting 6.5 million patients, and amasses the annual treatment costs to an excess of US$25 billion (Sen et al. 2009). And with a high, as well as increasing, prevalence of lifestyle diseases, we can expect a rise in this patient population.

1.2 The skin

The skin, our body's largest organ is a mechanical barrier and our first line defence against the environment. This is mostly due to the relatively impermeable epidermis, as permeability through the dermis is quite good. Something exhibited in patients with impaired skin; such as burn victims or chronic skin wound sufferers. The skin consists of three main layers: the outer epidermis, the inner dermis, and the innermost hypodermis - here called the subcutaneous tissue. These three layers can further be divided into several sub-layers **(**Figure 1**)** (Sherwood 2012; Venus et al. 2010).

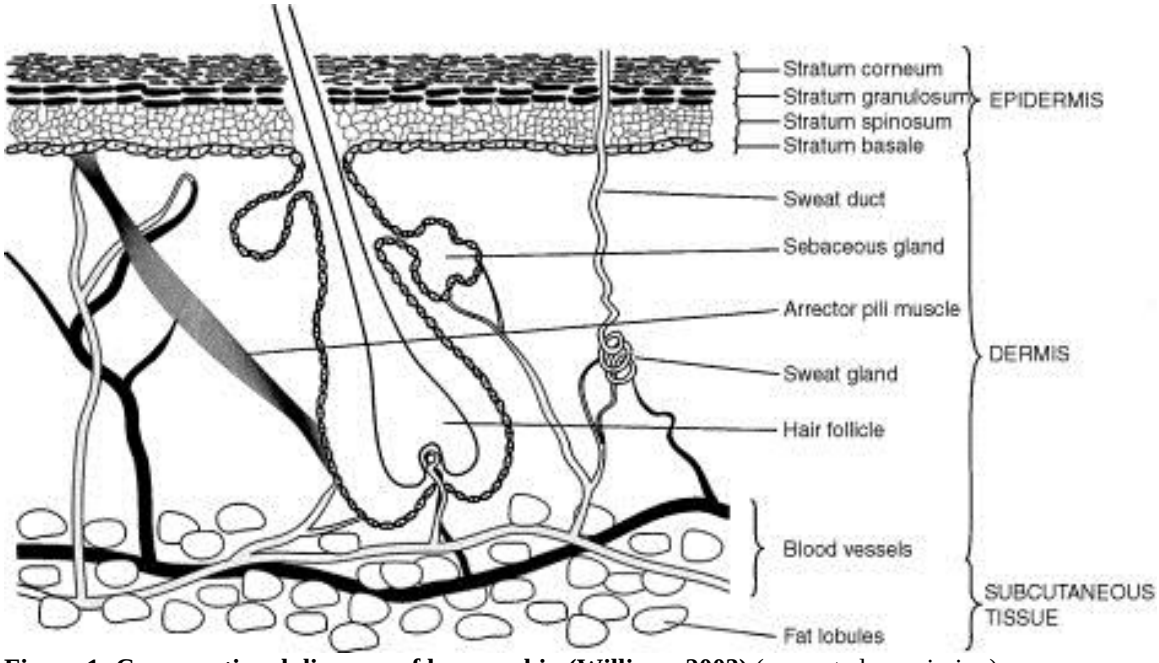

Figure 1: Cross-sectional diagram of human skin (Williams 2003) (requested permission).

1.2.1 Layering and functions

1.2.1.1 Epidermis

The epidermis is primarily comprised of keratinocytes and can be divided into four layers from the most outer to inner: *stratum corneum* (SC), stratum granulosum, stratum spinosum, and stratum basale. Respectively called the horny layer, the granular layer, the spinous layer, and the basal layer (Venus et al. 2010). Some may also include the stratum lucidum which places between the SC and the granular layer (El Maghraby et al. 2008). Literature may sometimes differentiates between the epidermis, and the viable epidermis excludes the SC resulting in a thickness of 50-100 μm (Bouwstra et al. 2006).

The SC is 10-20 μm thick and varies depending on the body localisation and the amount of "wear and tear", or cell abrasion (Hwa et al. 2011). It consists of keratinocytes that have been "shoved" from the granular cell layer by new forming cells. These displaced cells in the SC are now called corneocytes due to their loss of cytoplasmic organelles and nuclei, which cause them to have a flattened appearance as they only retain keratin and water before forming a strong and interconnected covering. Among other things this layer serves as a protection against microbes, chemicals, and loss of body water. Since the epidermis has no direct supply of blood the exchange of nutrients and waste products happens through diffusion through the dermis (Bouwstra et al. 2006; Sherwood 2012). The SC is also known to be the rate-limiting step in transdermal permeation of most molecules (El Maghraby et al. 2008).

The granular layer's function is mainly cell adhesion, cytokine production via keratinocytes, production of vitamin D, and keratin production. While basal cell layer is relatively thin, at around one to three cells in thickness it plays a vital role through cell repair and proliferation (Venus et al. 2010).

1.2.1.2 Dermis and hypodermis

The dermis is a connective tissue layer at about 3000-5000 μm thick. It consists of elastin and collagen fibers embedded in an aqueous gel containing salts and glycosaminoglycan. The dermis also contains copious amounts of capillary vessels and specialized nerve endings, as well as lymphatic vessels (El Maghraby et al. 2008; Sherwood 2012).

The elastin makes the skin elastic and flexible, whereas collagen gives it tensile strength. The blood vessels play two important bodily roles: nutrient supply, as discussed earlier, and

temperature control by the means of heat exchange. The peripheral nerve endings can be split into two groups: the efferent and afferent. The efferent ones detect pain (nociceptors), temperature, pressure (Pacinian corpuscle, Ruffini endings), and other somatosensory input (hair receptor, Merkel's disc, Meissner's corpuscle)(Hoffmann et al. 2004; Sherwood 2012).

Hair follicles, sebaceous glands, and apocrine and eccrine (primarily for thermoregulation) sweat glands are the different appendages originating in the dermis (Cui et al. 2015). Hair follicles, which account for 0.1% of the entire skin surface, have sebaceous glands attached to their shaft that secrets sebum which lubricates and helps the skin maintain a pH 4.5-5.5. Sebum consists of triglycerides, free fatty acids, wax esters, squalene, and sterols (Benson et al. 2012; Otberg et al. 2004; Scharschmidt et al. 2013). This in conjunction with eccrine sweat, which also lowers the pH and expresses several antimicrobial peptides (AMPs), contributes to make the skin relatively inhospitable (Sanford et al. 2013). Literature also reports the pH in the range of 4.5-5.5 (Goering et al. 2012; Lee et al. 2006).

The hypodermis situated below the dermis serves as an anchor for the skin. Most of the adipose tissue is located here, where it functions as energy storage, insulation and protective padding. Nearly 80% of adipose tissue is found in this layer in non-obese subjects (Hwa et al. 2011; Lai-Cheong et al. 2009).

1.2.2 Microbiome

Having discussed the skin composition and its function as a mechanical protective barrier, we will now examine the role of the different microorganism that inhabit the skin's surface and how they work in synergy with our innate defences.

Despite being a relatively hostile environment the skin is host to a rich and assorted population of microorganisms. About 10^6 bacteria reside on every square inch of our skin, most in the surface layer of the SC, whereas the SC layer bordering to the stratum granulosum contains scarce quantities of bacteria. This colonisation is labelled as the skin 'microbiome' or 'microbiota', which includes bacteria, fungi, viruses, archaea and microeukaryotes. These microorganisms occupy various body environments like the oral cavity, skin, and gut while specializing in their distinct niches suitable for a certain location(Hannigan et al. 2013; Scharschmidt et al. 2013). One of the important advantages of having the commensal

microbiome is preventing colonization and/or invasion by opportunistic or pathogenic species (Goering et al. 2012).

1.2.2.1 Homeostasis

Foetal skin is regarded as sterile up until birth, after which colonization occurs and continually develops while being affected by body topography, occupation, geographical location, gender, age, maturation, environment, and other factors before eventually reaching homeostasis (Zeeuwen et al. 2013).

Upon reaching homeostasis certain microorganisms will be more dominant than others. The four prevalent phyla found in the skin are: *Actinobacteria, Firmicutes, Proteobacteria, and Bacteroidetes.* Within these phyla are the three most common bacteria genera, which are: *Staphylococcus, Corynebacterium, and Propionibacterium*. The former being in the *Firmicutes* phylum, while the two latter are in the *Actinobacteria*. *Propionibacterium* thrives and has the greatest presence in sebaceous regions, such as the back, while *Corynebacterium* and *Staphylococcus* colonize moist regions, such as the armpit (Figure 2**)**. All of the areas were subjected to interpersonal variety and temporal fluctuations, although to a even greater magnitude in the drier and more exposed skin regions (Chen et al. 2013).

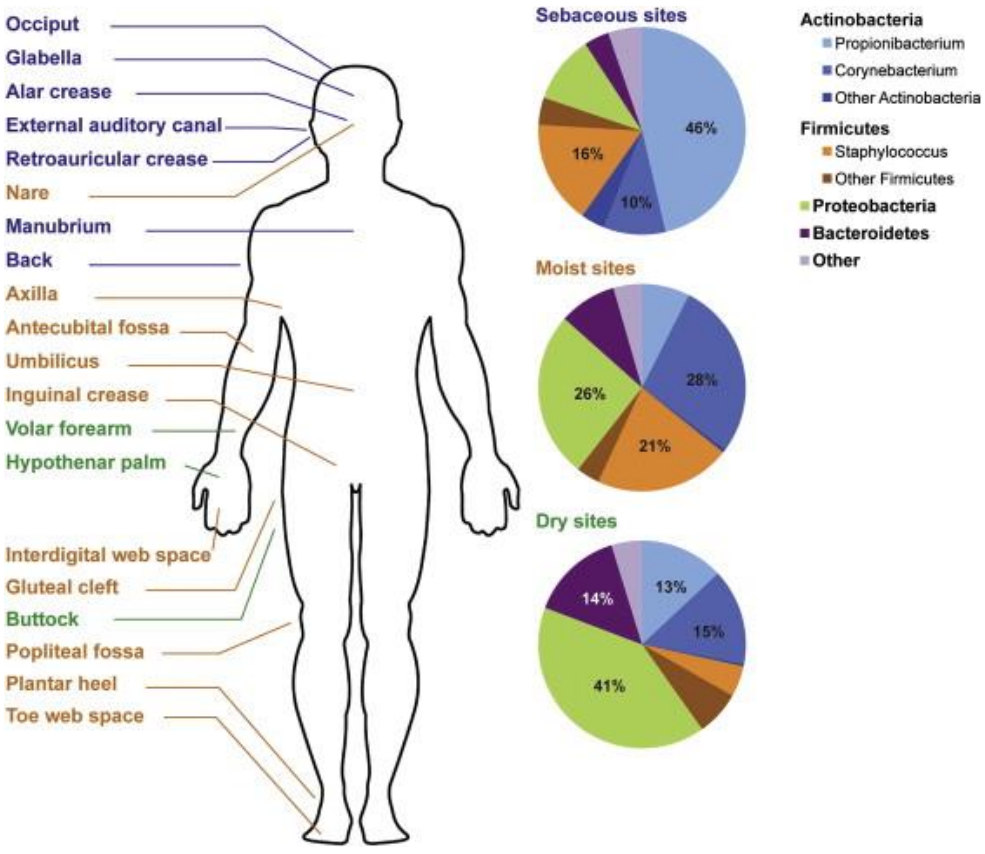

Figure 2: Microbiome distribution on the skin of a normal human being (Chen et al. 2013) (with permission)**.**

1.2.3 Wounds

A wound may be considered to be a break or a flaw to the skin's normal integrity, thus making us more susceptible to environmental harm or pathogens as the skin barrier has been compromised (Broughton et al. 2006). Wounds are usually classified as either acute or chronic depending on the reparation process. Acute wounds generally heal to completion, with minimal scarification, inside the period of 8-12 weeks. Acute wounds may be caused by mechanical, burn, and/or chemical injuries. Most common are the mechanical injuries such as abrasions, or penetrating wounds (e.g. gun shot, knives). Chronic wounds however, occur due to slow and incomplete healing tissue injuries that exceed the time span of 12 weeks and repeatedly return because of underlying ailments. Such as diabetic foot ulcers and pressure ulcers (Boateng et al. 2008).

1.2.3.1 Healing process

Wound healing is a complex process and is usually divided into four separate phases: (1) coagulation and haemostasis, (2) inflammation, (3) proliferation, and (4) the remodelling phase (Velnar et al. 2009).

The first stage starts immediately after an injury, and is completed in the matter of hours. Shortly after this, comes the second stage that is finalized within 24 hours to 7 days after the incident. Then third and the major repair stage follows, which takes place 1-3 weeks after the injury. The final stage starts around 3 weeks after the occurrence and varies from anywhere between months to several years (Strodtbeck 2001).

Instantly after the occurrence of an injury, the skin tries to minimize the loss of fluid and blood, as well as flushing potential microorganism out of the wound site. The blood coagulation happens via the extrinsic and intrinsic clotting pathway, which causes an accumulation of platelets resulting in vasoconstriction. Thereafter fibrin and fibronectin are engaged and form a clot that acts as a temporary seal over the wound site protecting it from the invasion of foreign matter, stops further bleeding, and acts as a matrix for fibroblast, neutrophil, and keratinocyte migration in the following phases (Shaw et al. 2009; Strodtbeck 2001).

The inflammatory response phase is initiated by different intermediaries at the wound site. Neutrophils arrive shortly after the injury and are tasked with preventing infection by containing potential pathogens by phagocytosis for the first couple of days after the injury. Other white cells like monocytes, and lymphocytes are also attracted to the site, although neutrophils are the dominant cell type before slowly dissipating in absence of an infection (Figure 3**)**. Following this, the monocytes differentiate into macrophages and function as the main phagocytic cell at wound location during the rest of the healing process, where they will clear cellular remnants, dead neutrophils, and microorganisms, as well as secrete nitric oxide, which enhances vasodilation and permeation, and cytokines that initiate injury repair(Shaw et al. 2009; Strodtbeck 2001).

The proliferation phase (Figure 3) is where the new skin tissue is formed that covers the injury site. The establishment of new blood vessels, skin, and connective tissue, respectively neovascularization, re-epithelisation, and granulation, is vital for this process as they restore the skin's barrier function while supplying it with essential nutrients and oxygen. Tensile strength begins to take hold in this stage, but is not fully apparent until the fourth stage.

Neovascularization or angiogenesis is the restoration of the capillary network in the avascular wound cavity, and is induced by lactic acidosis and different growth factors. Some of which are thought to be due to a hypoxic environment.

The complete coverage of the wound site is referred to as re-epithelisation, where keratinocyte are the predominant cell type stimulated by growth factors and chemotaxis. The keratinocytes migrate by moving from the border of the wound by elongation and attachment to a new site until the movement concludes by "contract inhibition" which is when the two borders meet. The other mode of migration is when a certain cell has relocated 2 to 3 cell lengths, ceases activity and allows another cell to "climb over" it, a term referred to as leapfrogging.

The granulation is the closing mechanism of proliferation and repair, where the fibrin/fibronectin-containing blood clot is replaced by granulation tissue which is mediated by fibroblasts. This matrix is primarily composed of collagen, albeit distinctive varieties. Myofibroblast, differentiated fibroblasts, also contribute to the granulation process by contracting the wound (Shaw et al. 2009; Strodtbeck 2001).

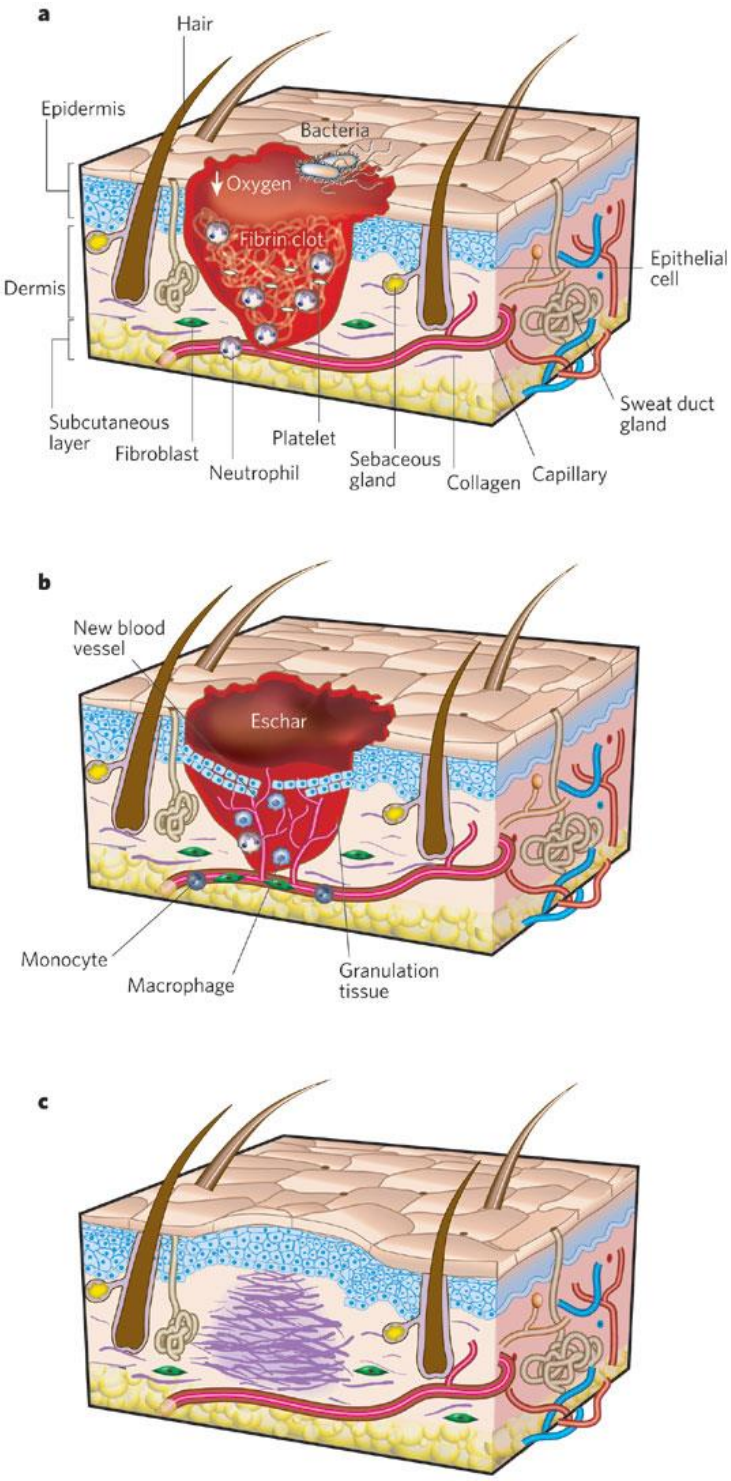

Figure 3 Phases of wound healing: a) Phase 1 & 2; haemostasis and inflammation, b) Phase 3; proliferation, c) Stage 4; remodelling (Gurtner et al. 2008) (with permission)**.**

Remodelling is the fourth and last wound healing process where the granulation tissue matures or scars, thus leaving an "ordinary" skin appearance as well regaining over 80% of its original skin tensile strength **(**Figure 3). During this process both the metabolic activity in the extra cellular matrix, and angiogenesis are steadily diminishing, apoptosis is initiated in

keratinocytes, fibroblast, and macrophages, as well as the existence of a fine equilibrium between the dismantling, synthesis, and thickening of collagen resulting in a stronger and functional skin tissue. The pitfall to this strengthening is that it makes the new skin less anchored to the underlying scaffold than unaffected skin. In addition to this epidermal appendages like hair orifices have difficulty being re-established in scarified tissue (Shaw et al. 2009; Strodtbeck 2001; Velnar et al. 2009).

1.2.3.2 Bacterial contaminations

Bacterial colonization is present in all wounds leading to an increase in inflammatory mediators such as free oxygen radicals, cytotoxic enzymes, and metalloproteinases, which consequently are believed to delay the wound healing by matrix degradation (Martin et al. 2010). However, Some literature argues that regular contamination does not contribute to impaired healing, and that one should differentiate healing impairment with regards to the extent of bacterial contamination and necessary treatment, also known as bioburden (Singh et al. 2013). Bacterial bioburden can be categorized into four distinct groups with increasing bacterial presence: 1) *contamination*, 2) *colonization*, 3) *critical colonization*, or 4) *infection*. Group 1)-2) do not elicit a host response, even though 2) has replicating bacterial strain, whereas 1) has not. It is first at 3) critical colonization, the amount of bacteria is high enough to cause damage to the resident tissue and may interfere with the wound healing. At 4) the bacteria have a strong foothold and elicit a host reaction (Singh et al. 2013).

The colonizing bacteria in chronic wounds stem from a wide range of locations such as: the vagina, local skin flora, the oral mucosa, and the external environment. Making the matter even worse is the genotypic expression of these bacteria making them readily form persistent communities that are embedded in a extrapolysaccharide matrix (EPM), better known as biofilms, making them less sensitive toward antibiotics and innate defences (Davies 2003; Martin et al. 2010). About 60% of chronic wounds are afflicted by biofilms, in comparison only about 6% of acute wounds are affected, and the most common bacterial families found are *Staphylociccaceae, Pseudomonadaceae, Stretococcaceae, Clostridiales Incertae Sedis XI, and Enterobacteriaceae* (James et al. 2008).

1.2.3.3 Biofilm

As previously mentioned biofilms enfolds the bacteria in a matrix made of polysaccharides, glycolipids, glycoproteins, proteins, and extracellular DNA matter from the microorganisms. The film can consist of several or a singular fungal of bacterial species that do not discriminate upon which surface the film is formed (living or inert) (O'Toole et al. 2000; Percival et al. 2015; Taraszkiewicz et al. 2013). The biofilms serves as an ideal milieu for the microbes, permitting avoidance from innate host defences, increased resistance to antibiotic treatment, as well as increasing cell survival rates (Demidova-Rice et al. 2012).

The formation of a biofilm can arbitrarily be split into three phases: early, intermediate, mature (Figure 4**)** The first stage involves migration or movement of the planktonic cell through passive transfer of body fluids or by the use of flagella. Thereafter, the microbes make contact with a surface and develop a single layer of cells, consequently not yet having activated their reduced susceptibility to antibiotics. The second step involves the formation of microcolonies, preceded by the irreversible surface binding, and concluded by the polymer matrix being formed and encasing the microbes. The third and the final step of biofilm formation is the establishment of a mature microbial population. It is during this stage the microbes might be liberated from their mushroom-shaped microcolonies, and transferred to another subsequently spreading the infection (Taraszkiewicz et al. 2013).

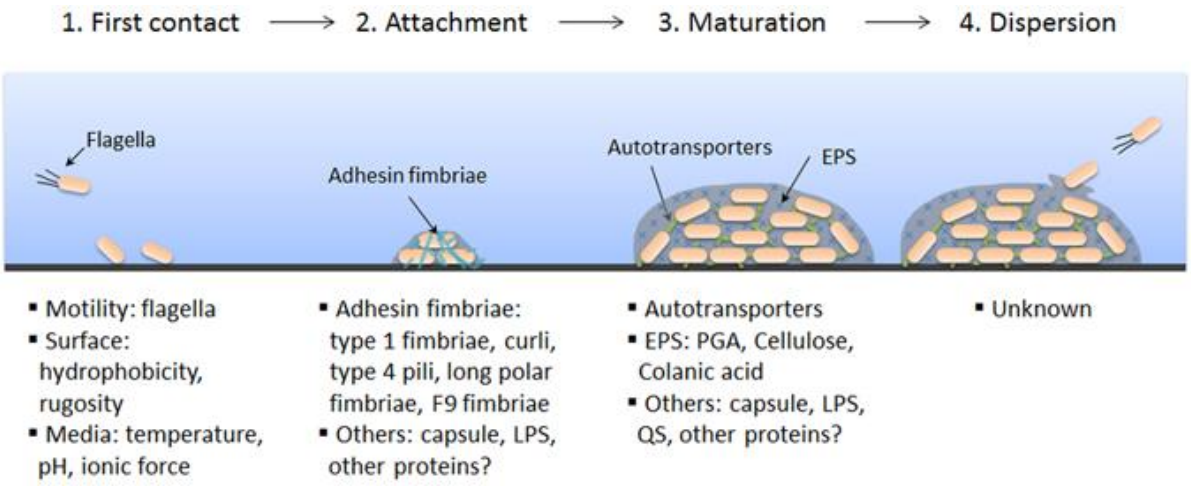

Figure 4 Stages of biofilm formation in a Shiga-toxin producing E-coli. Stage 1 is considered to be point 1 and 2 in this illustration. It should be notes that not all factors listed below the steps are applicable for other bacteria (Vogeleer et al. 2014) (with permission).

Among the various regulation mechanism of biofilm formation quorum sensing (QS) is the best revised. The mechanism entails the detection, production, and release of chemical signalling particles as a means of communication between the microbes. Acyl homoserine lactone (AHLs), ogliopeptides, and autoinducer-2 (AI-2) are three most common classes of QS signalling substances, where Gram-positive bacteria primarily use ogliopeptides while Gram-negative bacteria use AHLs.

1.3 Photodynamic therapy

Photodynamic therapy (PDT) is an optional clinically recognized treatment method for several diseases, which include different types of cancer (bladder, skin, colon), acne, and infections. The latter being of great interest due to the continuous increase of resistance in antimicrobial treatments (Cieplik et al. 2014). PDT consists of three main components: a chemical substance referred to as a photosensitizer (PS), a visible light source at a certain wavelength, and oxygen. The light activates the PS, which produces reactive oxygen species (ROS) that in turn result in a microbicidal effect by cellular damage or cell death (Bechet et al. 2008; Taraszkiewicz et al. 2013).

1.3.1 Photosensitizers

Several photosensitizers for PDT exist, and they are usually divided into three groups – prophyrins, chlorophylls, and dyes. These distinctive grouping is based on their accumulations site. PS are vessels that permit enable the transfer and translation of light into chemical reactions (Allison et al. 2004).

5 - aminolevulinic acid (ALA), a hydrophilic pro drug and in the prophyrins family, is a naturally occurring amino acid that converts to protoporhyrin IX (PpIX) in the haem biosynthesis by a reaction between glycine and succinyl-CoA (Figure 5). The reaction takes place in the mitochondria and is catalysed by the enzyme ALA synthase (ALAS), before reaching the cytosol. The cofactor pyridoxal-5-phosphate (PLP) is also required for the reaction to occur. While in the cytosol numerous reactions take place mostly facilitated by enzymes leading to the formation of coproporhyrinogen III (CPIII). CPIII is then transported back inside the mitochondria by peripheral-type benzodiazepine receptors (PBR), where coproporhyrinogen oxidase (CPO) serves as a catalyst in converting CPIII to protoporphyrinogen IX (PROTOIX). Fad-containing protoporphyrinogen oxidase (PPO), a catalyst, then coverts PROTOIX to PpIX; our photodynamic therapy target. Ferrochelatase, an enzyme, completes the biosynthesis pathway by inserting Fe^{2+} into PpIX resulting in the formation of haem (Valenta et al. 2005; Wachowska et al. 2011)

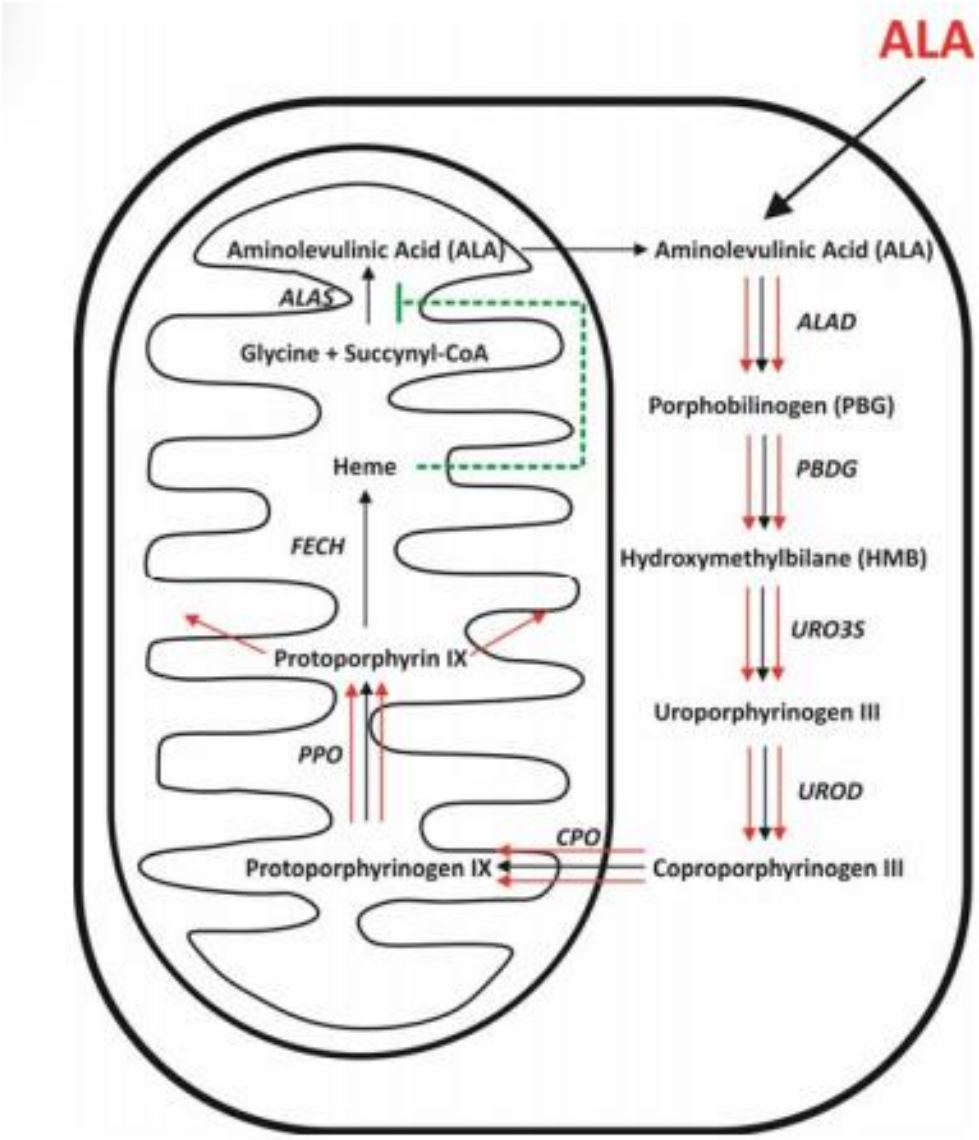

Figure 5: Overview of the haem biosynthesis pathway showing the different steps and converting enzymes (Wachowska et al. 2011) (with permission).

In the haem biosynthesis pathway there are two rate-limiting enzyme: ALAS and ferrochelatase. These contribute to the regulation of PpIX through negative feedback mechanisms. However when exogenous 5- ALA is administered, it bypasses this mechanism leading to an accumulation of PpIX. A similar phenomenon is observed in cancer cells due to their lower iron concentrations and decreased ferrochelatase activity. Other factors that may affect the site accumulation of PpIX include lighting conditions, pH, and oxygen accessibility (Fotinos et al. 2006; Wachowska et al. 2011).

5-ALA **(**Figure 6) has challenging physiochemical properties such as low oral bioavailability, poor tissue penetration and non-homogenous PpIX distribution after topical application, in order for it to be used effectively in clinical settings. This is due to more than 90% of 5-ALA being present as a zwitterion under physiological conditions. These challenges have been combated by creating more lipophilic 5-ALA derivatives, where two of the most promising are the esters: methylaminolevulinate (MAL), and hexaminolevulinate (HAL). Respectively marketed as Metvix®(actinic keratosis and nodular/superficial basal cell carcinoma) and Hexvix®(optical imaging agent for bladder cancer), and both are developed by Photocure ASA (Fotinos et al. 2006). In addition to this the current market also has FDA approved Levulan® Kerastick® (actinic keratosis), and EMA approved Ameluz®(actinic keratosis), and Gliolan®(visualization of malignant glioma tissue during surgery).

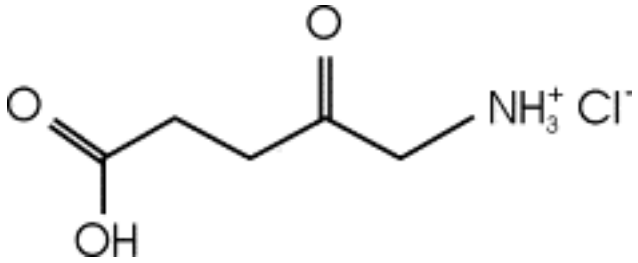

Figure 6: Chemical structure of 5-ALA. Clearly showing the amine and carboxylic terminal that under physiological conditions will both be charged.

1.3.2 Photochemical reactions

After applying light in the correct wavelength range to the PS it reaches a state of excitation capable of reacting with oxygen. This energy is then transmitted to either O_2 or biomolecules depending on the reaction pathway. The *type 1* (Figure 7**)** reaction involves electron transfer from the excited state to substrate, such as unsaturated membrane phospholipids, which leads to water-derived hydroxyl radicals (**HO•**) or lipid-derived radicals. These two radicals can combine or react with other biomolecules and oxygen to produce H_2O_2, which contributes to formation lipid peroxidation or ROS results in cell death or damage.

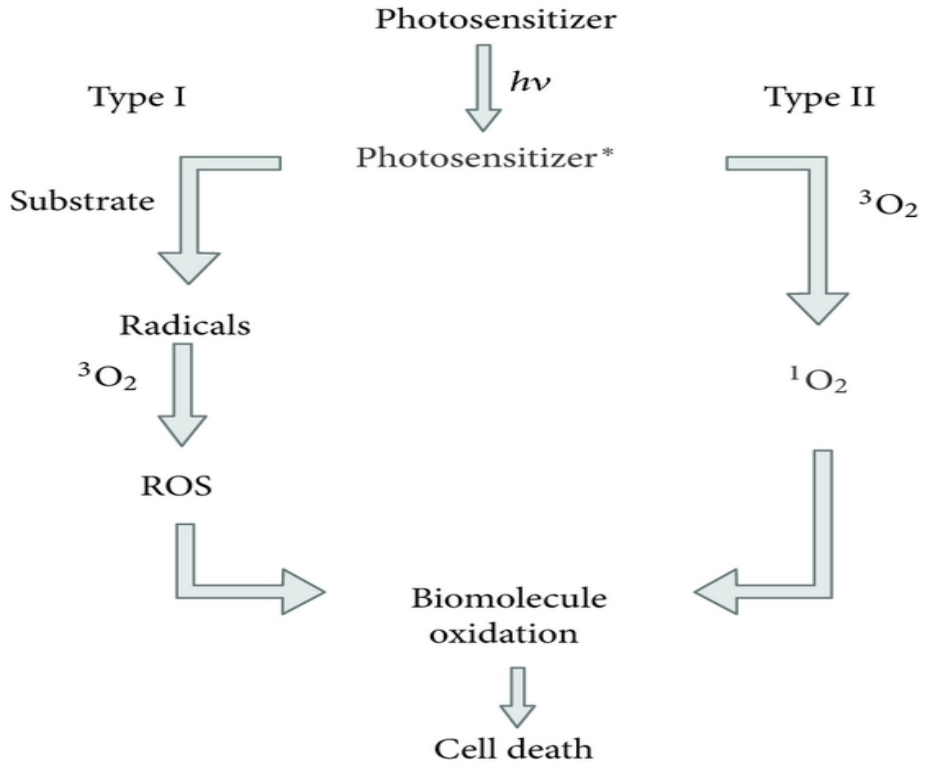

Figure 7: Scheme of the two pathways of the photodynamic process both resulting in cell death (Taraszkiewicz et al. 2013) (with permission).

Type 2 reactions produce singlet-state oxygen ($^1O_2$) by energy transfer from $^3O_2$ to O_2. $^1O_2$ is a highly reactive species that is able to cause the same cell death or damage by oxidizing cell biomolecules such as nucleic acid, proteins, and lipids. Although both of these reactions happen at the same time, type 2 is considered as the major contributor with regards to antimicrobial photodynamic therapy (aPDT) (Taraszkiewicz et al. 2013).

1.4 NCE

Photocure ASA provided the master student of 2014 with all the information about the new chemical entity (NCE) (Hadafow 2014; Hemmingsen 2015; Thoresen 2014).

NCE is a derivative of 5-ALA, and is expected to act in a similar manner as 5-ALA and other 5-ALA derivatives. It is soluble in water (3.6g/g water), and has a free amino group that has a pKa of around 8.3. It is highly unstable in aqueous solutions, and is readily degraded by hydrolysis.

1.5 Nanoparticles

Nanoparticles (NP) or nanotechnology as a concept is believed to have originated by a speech held by physicist Richard Feynman in 1959. Awareness around nanotechnology likely has been around for a longer period of time (Buzea et al. 2007; Oberdörster et al. 2007), however it was first used by Professor Norio Taniguchi in a paper in 1974 (Webster 2007). The field is still growing and the potential is seemingly vast.

The range of nanoparticles is between 1-1000nm (Buzea et al. 2007; Cornelia et al. 2015), although some discrepancy exists with regards to the exact range of what can be viewed of pertaining to the nanoscale. Some argue that particles in the size of 1-100nm are the 'true' nanoparticles, while others claim that anything submicronic could be considered to be of a nano size order.

The main purpose of creating NPs is to control the surface properties, particle size, and release of the active pharmaceutical ingredient as a means to achieve site-specific action of the API at an ideal rate and dose regimen. Nanoparticles can be made from various materials including polysaccharides, synthetic polymers, and proteins. The choice of the material depends on several factors such as: 1) required size; 2) drug properties e.g. stability and lipophilicity/hydrophilicity; 3) surface characteristics e.g. permeability and charge; 4) biocompatibility, biodegradability, and toxicity; 5) desired drug release profile; and 6) antigenicity of the final product (Mohanraj et al. 2007).

The three methods that predominate nanoparticle preparation are:

a) *Polymerization of monomers:*
This method is based upon the polymerization of monomers to form nanoparticles in an aqueous solution. The drug loading is performed by adsorption onto NPs after the polymer is formed or by dissolving the drug in the medium pre-polymerization. The NP suspension is then subjected to purification, and re-suspended in an isotonic surfactant free medium. Particle size and capsule formation is dependent on stabilizer and surfactant concentration. Polybutylcyanoacrylate can be prepared by this method.

b) *Dispersion of preformed polymers*:
This method can be performed by either the 1) *solvent evaporation method* or the 2) *solvent diffusion method*. In the 1) solvent evaporation method a polymer is dissolved in an organic solvent such as chloroform or dichloromethane and emulsified in an aqueous solution in order to form an oil-in-water emulsion. After the emulsion has stabilized continuous stirring or a pressure reduction vaporizes the organic solvent. The stabilizer and polymer concentration, as well as the homogenizer speed affect the particle size. Small particle size may be produced by ultrasonication or high-speed homogenization. 2) The NPs in the solvent diffusion method are formed by the interfacial turbulence between a water-miscible solvent and a small amount of water immiscible organic solvent. The size is affected by the concentration of the water-miscible solvent, and as the concentration of this solvent increases the particle size decreases. Both methods have been found to be suitable for hydrophilic and hydrophobic drugs. Common polymers used in these methods include polylactic acid (PLA), polyglycolic acid (PGA), poly lactic-co-glycolic acid (PLGA), and polycyanoacrylate (PCA).

c) *Ionic gelation or coacervation of hydrophilic polymers*:
This method consists of two aqueous phases, chitosan (cationic) and polyanion sodium tripolyphosphate (anionic), being mixed together and forming nanosized coacervates due to the electrostatic interactions. Ionic gelation on the other hand involves materials transitioning from liquid to gel at room temperature due to ionic interactions (Mohanraj et al. 2007). The formation of coacervates is similar to that of the supra-molecular self-organizing chitosan/lecithin NPs used in this project, which also are formed due to ionic interactions(Sonvico et al. 2006).

However, other preparation methods are also possible such as the particle replication in non-wetting templates, and supercritical fluid technology (Mohanraj et al. 2007; Pal et al. 2011).

1.5.1.1 Nanoparticles as a drug delivery system

Nanoparticles are known to have advantageous controlled release properties, as well as increasing the stability of proteins and/or drugs. The benefits of using NPs as a drug delivery system include:

1) Manipulation of size and surface characteristics in order to attain active and passive drug targeting after administering the NPs parentally; 2) controlling and sustaining the drug release during transportation and at the delivery site, thus altering drug distribution in the clearance, which results in increased efficacy and reduced side effects; 3) particle degradation and controlled release properties can be altered by matrix choice. The drug load is relatively high, and effortless (no chemical reaction is needed) which preserves the drug activity; 4) active targeting can be attained by ligand attachment or by external guidance with a magnet; 5) several routes of administration can be used such as parenteral, dermal, nasal, or oral.

Although the listed advantages are quite beneficial, there are however some disadvantages such particle aggregation, burst release, and a limited drug loading capacity due to the small size (Mohanraj et al. 2007).

The hydrophobic nature of most PDT agents causes them to aggregate in aqueous environments, leading to interactions that can affect solubility, and radical species formation. Encapsulating the PDT agent would improve these shortcomings, as well as others by increasing target specificity and photostability, improved biodegradability, being non-immunogenic, as well as protecting the PDT agent from degradation(Bechet et al. 2008). Nevertheless, there are also disadvantages of colloidal drug carriers like difficulties of scaling up, limited stability in solution, and the use of organic solvents (Sonvico et al. 2006).

1.5.1.2 Specific characteristics for skin delivery

Local and systemic drug delivery can be achieved by different measures, whereas the skin is one of the routes that have been used for quite some time. Topical administration of dissimilar substances have been present throughout the times, but it was first in the 1970's that systemic delivery was an established method by the introduction of transdermal patches (El Maghraby et al. 2008). The clearest advantages to dermal and transdermal delivery are circumventing challenges that are present in the gastrointestinal tract, and first pass metabolic effect (Maghraby et al. 2006). An optimal size for nanocarriers with skin destination is also a disputable topic, but 200-300nm is acceptable (Hurler et al. 2012).

Any compound applied to the skin has two main crossing passageways: the transappendagael or the transepidermal pathways. Respectively also know as the intercellular or transcellular pathway **(**Figure 8). The brick and mortar model of the SC is also clearly observed in the figure.

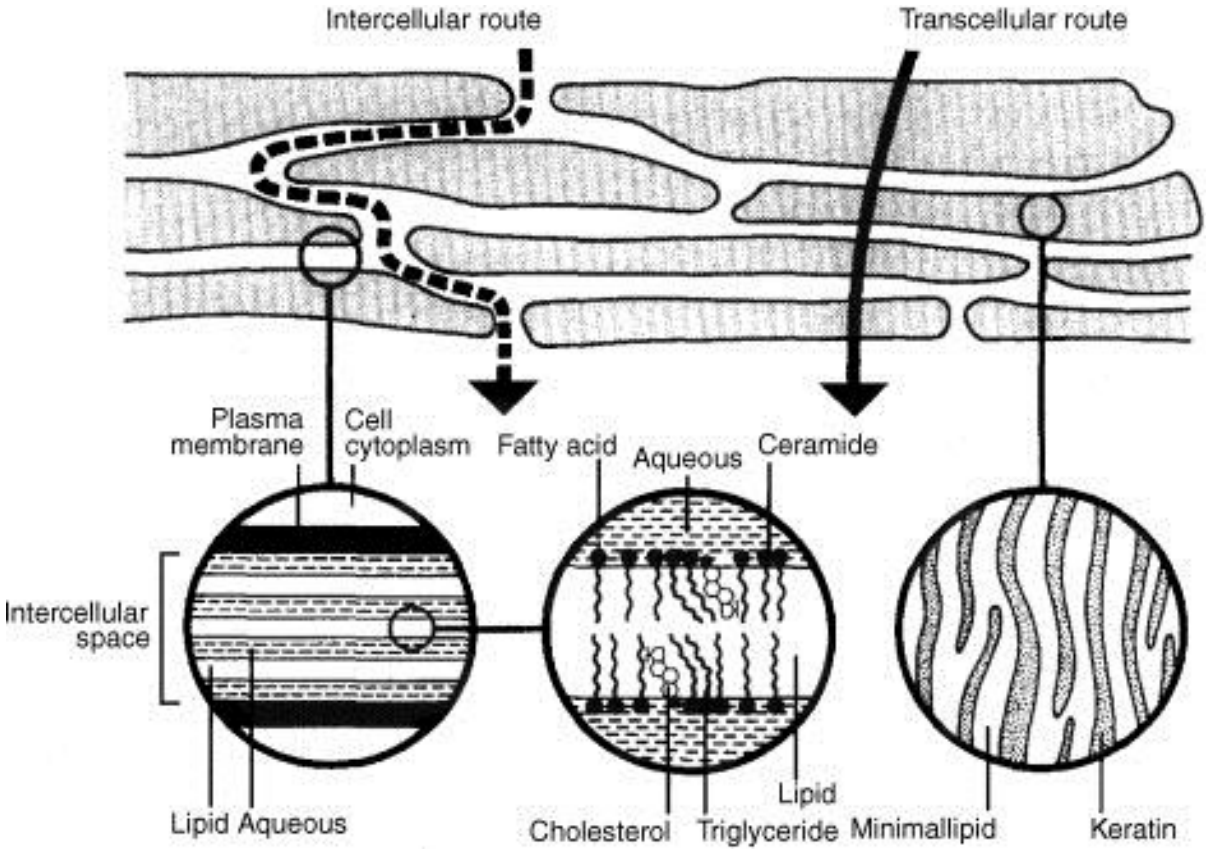

Figure 8: Human skin permeation through the intercellular or the transcellular pathway(El Maghraby et al. 2008) (with permission).

Substances that permeate intact, as well as hydrophilic of polar compounds, across the skin are thought to use the transcellular pathway. Contrary, lipophilic drugs prefer the intercellular pathway due to the lipid lamellae. The intercellular pathway is thought to be the main route of entry through the SC (El Maghraby et al. 2008; Hwa et al. 2011).

A third route namely follicular penetration has also been proposed **(**Figure 9). Though, due to the fact that follicular orifices only account for 0.1% of the entire skin surface, this pathway has until recently been ignored (El Maghraby et al. 2008; Uchechi et al. 2014).

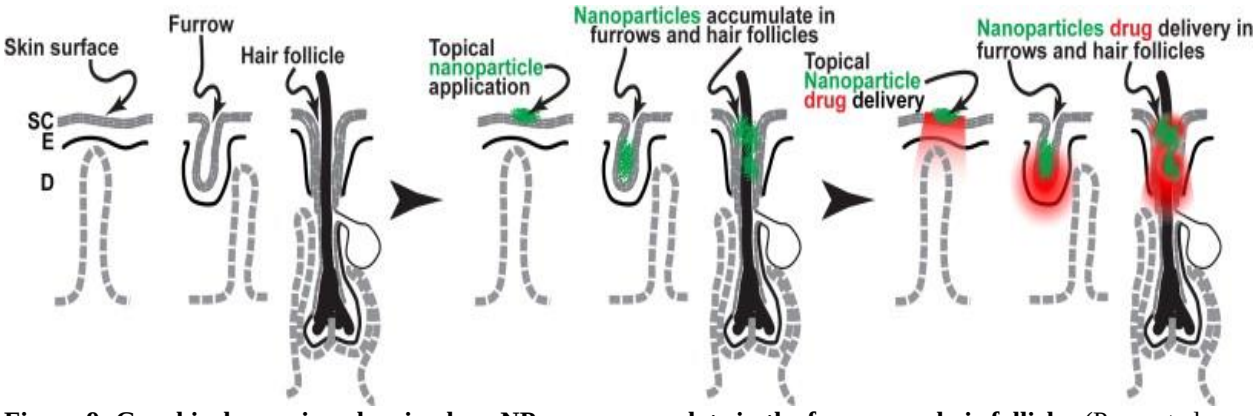

Figure 9: Graphical overview showing how NPs can accumulate in the furrows or hair follicles (Prow et al. 2011) (with permission).

A selection of studies has shown that this third route may be viable for formulations with a smaller particle size (Kimura et al. 2012; Prow et al. 2011; Uchechi et al. 2014), However larger particles (around 600nm) are of particular interest with regards to topical vaccinations, this due to large concentration of Langerhans cells around the follicles (Witting et al. 2015).

1.5.2 Chitosan

Chitosan is a linear cationic polysaccharide made of the copolymers glucosamine and N-acetyl-D-glucosamine that are linked by β-(1-4)-bond (Figure 10), and has a pKa at around 6.5 making it insoluble at higher pH values (Pelgrift et al. 2013; Zhang et al. 2010). It a derivative of chitin, a naturally abundant polysaccharide found in exoskeleton crustaceans and arthropods. The degree of deacetylation (DD), and molecular weight (MW) are two factors that influence chitosan properties (Jayakumar et al. 2010; Ravi Kumar 2000).

Chitosan has MWs stretching from 50-2000kDa, and DD between 40-98%. Chitosan can be grouped into low MW and high MW. Low MW chitosan is considered to have MW between

20-190kDa and a DD less than 75%, while high MW chitosan is 190-375kDa and a DD above 75% (Baldrick 2010; Dash et al. 2011; Seyfarth et al. 2008).

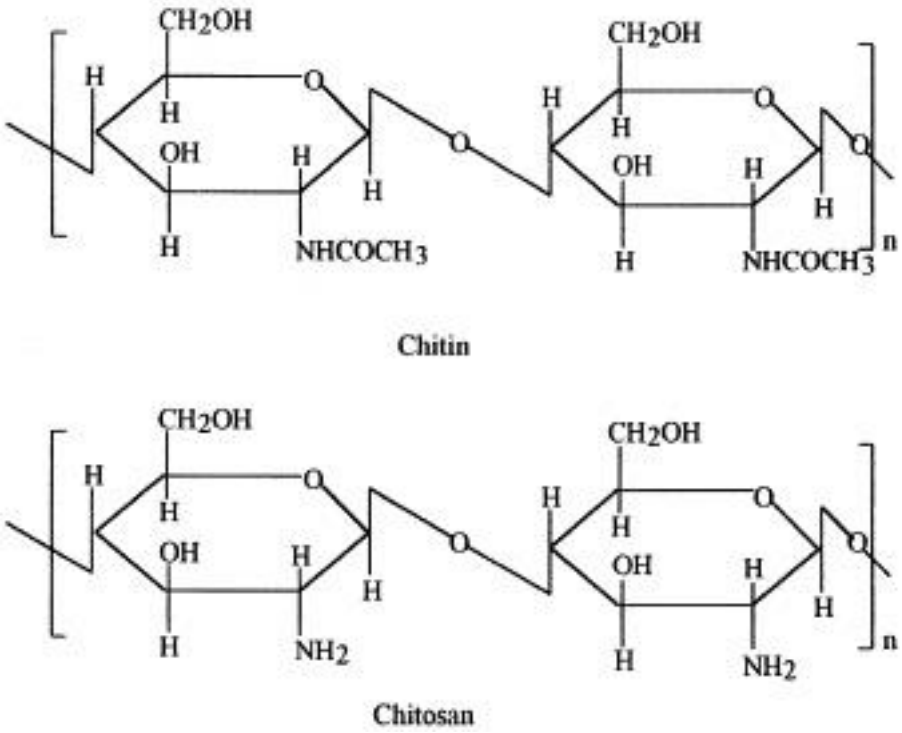

Figure 10: Chemical structure of cellulose, chitin, and chitosan (adapted from (Ravi Kumar 2000) (with permission)).

For instance, an increase DD and MW results in increased solubility, mucoadhesion, and antimicrobial effect, while the opposite is true for biodegradability (Dash et al. 2011).

1.5.2.1 Properties of chitosan

Chitosan is considered to be biocompatible, mucoadhesive, low to non-toxic, antibacterial and antifungal, as well as have low immunogenicity. It is also generally recognized as safe (GRAS) in the food industry in the US (Baldrick 2010; Dash et al. 2011).

The antimicrobial properties of chitosan are of special interest to this project as they can work in synergy with 5-ALA. Chitosan's antimicrobial properties are thought to have various mechanisms of action making potential resistance unlikely. This includes: 1) ionic interaction (given pH values lower than pKA) between the cationic chitosan and the anionic plasma membranes and cell walls of bacteria, 2) DNA binding to fungal and bacterial cells, thus

inhibiting mRNA translation, 3) metal chelation, consequently reducing metalloprotein activity, and 4) Increased wound healing by inhibition of proinflammatory cytokines and recruitment of fibroblasts. All these properties may be increased to a further extent by incorporating chitosan into NPs. NPs comprised of low MW chitosan have proven to a greater effect against Gram negative bacteria due to them being more negatively charged, while high MW chitosan better affects Gram positive bacteria (Croisier et al. 2013; Pelgrift et al. 2013).

1.5.3 Lecithin

Lecithin is a mixture of phospholipid found in soybeans or egg yolks. The predominant types of phospholipids (PLs) that are present in lecithin are phosphatidylcholine (PC) (Figure 11), phophatidylethanomine (PE), and phosphatidylinositol (PI) (Xu et al. 2011). Lecithin is regarded to be safe and biocompatible, and has previously been used in liposomes and several nano delivery systems such as solid lipid nanoparticles (Hafner et al. 2011; Sonvico et al. 2006).

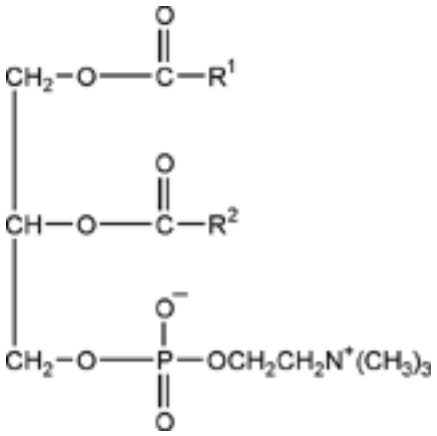

Figure 11: Chemical structure of alpha-phosphatidylcholine. The R groups are fatty acids that can be similar or dissimilar (Shah et al. 2015) (with permission).

1.6 Nanotoxicology

Nanomedicine is a field in exponential growth, however concerns arise due to both potential environmental and health hazards based on the same factors making it useful within medicine; surface modifications and size. Thus creating a new subdivision within the world of toxicology; nanotoxicology (Buzea et al. 2007). Nanotoxicology pertains to the biokinetic assessment of engineered nanodevices and nanostructures. Physiochemical properties such as physical absorption ability, and chemical reactivity are directly linked to the particle size and determine *in vivo* nanotoxicological behaviour (El-Ansary et al. 2009). Other aspects that should be taken into consideration are: biodistribution, routes of exposure, regulatory aspects, and genotoxicity (Figure 12**)** (Arora et al. 2012).

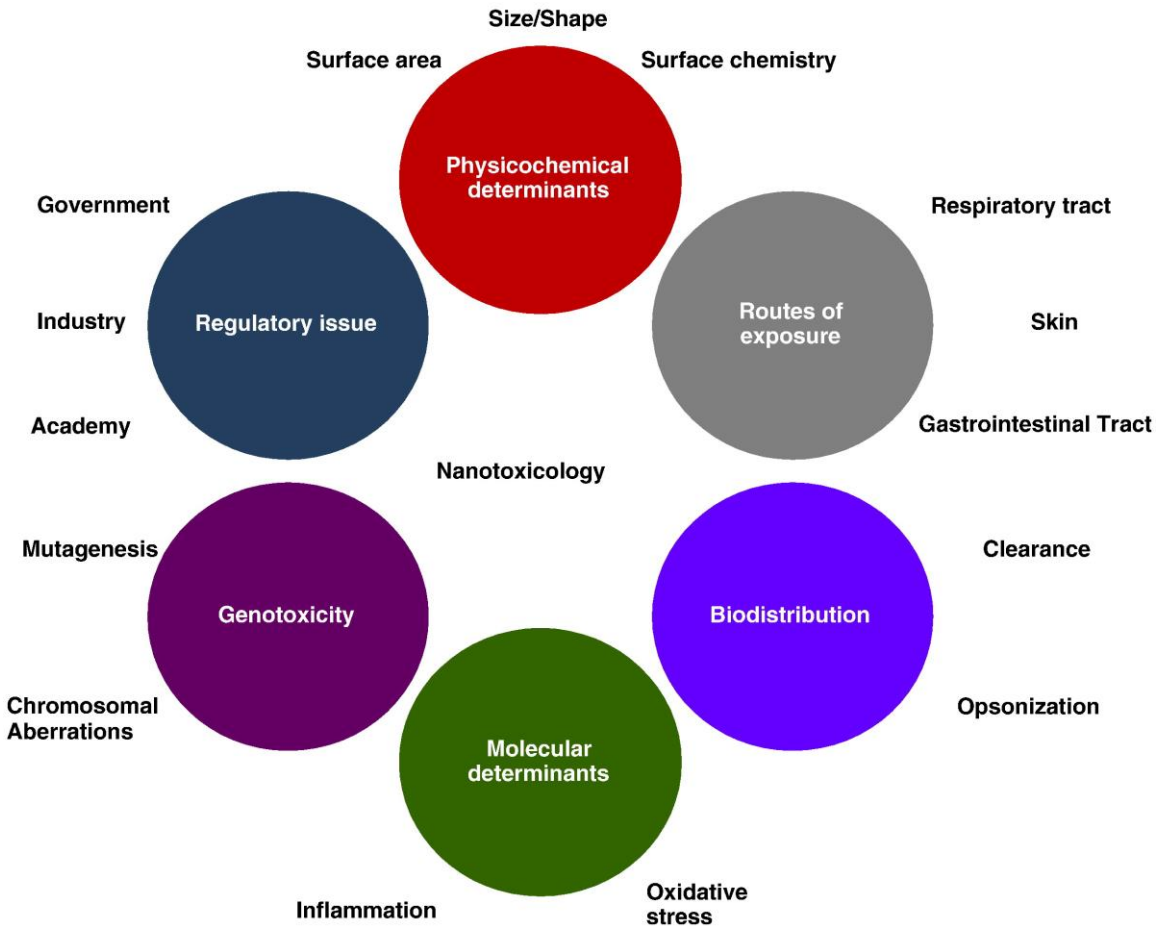

Figure 12 Overview of toxicity issues surrounding nanoparticles (Arora et al. 2012) (with permission).

As previously mentioned the physiochemical characteristic of nanomaterials determine the exerted biological effects. Other properties that should be taken into consideration are: chemical composition (crystallinity, purity, etc.), solubility, aggregation, shape, and surface structure (surface groups, inorganic or organic coatings, surface reactivity, etc.). The increased surface area is linked to the potential number of groups on the particle surface that may be involved in reactions with biological tissue (Arora et al. 2012).

In a study gold NPs at 15 nm were found to affect the biodistribution, whereas gold NPs at both 15 and 50 nm showed blood brain barrier permeability. Studies also showed that anionic NPs at lower concentrations were found to have higher uptake rates in comparison to cationic or neutral NPs at the same concentration, while cationic NPs were found to exhibit toxic effect at the blood brain barrier. Both studies were performed in rats. The shape of nanoparticles have been reported to affect biological activity. Spherical gold NPs were found to have a greater uptake compared to gold nanorods in HeLa cells, while NPs of a silver composition displayed shape-dependent interaction with *E. coli*. Length has also been proposed as an important aspect to consider in view of antase TiO_2 nanomaterials. Here alveolar macrophage inflammation has been initiated by toxic particles caused by the modifications of fiber structures larger than 15 μm (Arora et al. 2012). Surface charge was shown to be another important factor while assessing biological interactions. Neutral and charged gold NPs at 1.5 nm were respectively shown to lead to necrosis and cause cell death through apoptosis in HaCaT cells (Arora et al. 2012; Schaeublin et al. 2011).

The body has many partially open exposure sites able to interact with substances found in the environment e.g. the respiratory tract, the gastrointestinal tract, and the skin. The latter being of interest to our project. As extensively discussed in previous sections the skin serves as a protective penetration barrier against potential environmental hazards in varying size. However, skin nanomaterial exposure can also be intentional as in topical drug treatments.

A study performed with nanocrystalline titanium dioxide and magnesium oxide (as water suspension, dry powder, and water/surfactant suspension) on human dermatomed skin showed no dermal absorption after 8 hours due to an intact and functional *stratum corneum*. In a study performed with titanium oxide NPs at 20-100nm in human graft-, porcine-, and healthy human-skin reported a penetration limited to the 3-5 outermost corneocytes of the SC. However, other studies have shown greater skin penetration, some even reported NP accumulation in the dermis. Further, penetration of the intact SC resulting in dermal and epidermal accumulation has been reported for quantum dots with assorted physicochemical properties. Fullerene amino acid peptide NPs have also been shown to penetrate intact skin, with penetration reaching the dermis after mechanical flexion of the skin. In a study performed on epidermal keratinocytes with a variety of developed gold NPs were found to be non-toxic, while gold nanorods caused apoptosis. Inflammatory responses were initiated after the phagocytosis of the NPs by the keratinocytes. Cell toxicity in keratinocytes and fibroblasts has been demonstrated towards certain types of NPs such as nanoscale titania, single- and multi-wall carbon nanotubes, and quantum dots with surface coating (Arora et al. 2012). In addition, some studies with cobalt-chromium NPs have reported damage towards fibroblasts across an intact cellular barrier without penetrating it, which shows that direct contact with the cell or cellular uptake is not necessary in order to exert cytotoxic effects (Andón et al. 2014).

Nanoparticles exposed to transition metals or light may encourage the development of pro-oxidants and lead to the disruption of the equilibrium present in biological systems, which controls the detoxification and production of ROS. Shape, aggregation, and size are nanomaterial properties that can end the formation of ROS, while characteristics such as solubility and surface coating could either amplify or decrease the size effect (Figure 13) (Arora et al. 2012).

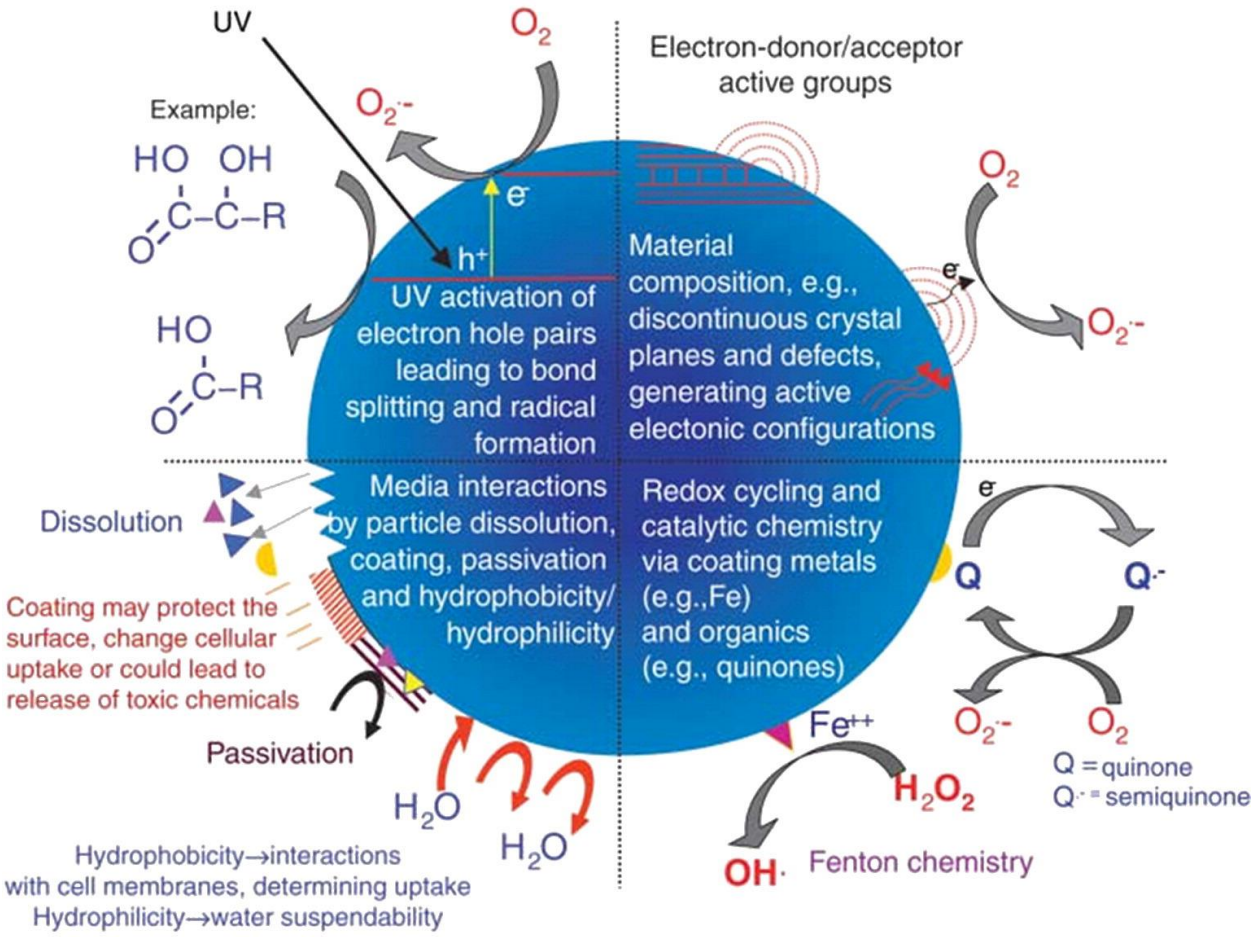

Figure 13 Overview of possible interaction between nanomaterials and biological tissue (Arora et al. 2012) (with permission).

ROS and the non-radical hydrogen peroxide (H_2O_2) are continuously formed in cells under normal conditions due to aerobic metabolism. This is a result of any stress or abuse that the cell is exposed to, and it can be of a physical or chemical manner. Mammalian cells are however equipped with an antioxidant defence system to counteract ROS either indirectly via reversing oxidative harm, or by intercepting directly. These systems can be grouped into two defence mechanisms: primary (catalase, superoxide dismutase, glutathione peroxidase, and thioredoxin reductase) or secondary (reduced glutathione). Superoxide dismutase converts

reactive radicals to the less reactive H_2O_2, which in turn is converted to O_2 and water by catalase, or reduced by glutathione peroxidase, resulting in protection against oxidative damage and reduced amounts of cellular lipid hydroperoxides. Free radicals produce lipid hydroperoxides, which cause damage, by attacking free fatty acids in the cell membranes. Whereas NPs are observed to increase inflammation through up regulation of proinflammatory mediators e.g. extracellular signal regulated kinases c-Jun, nuclear factor kappa β, and activating protein 1. NPs have also been reported to cause ROS generation, DNA damage, and oxidative stress, although in general the potential pathological consequences are limited to: necrosis, apoptosis, fibrosis, hypertrophy, metaplasia, fibrosis, carcinogenesis, and inflammation as previously mentioned. In order to evaluate the pathophysiological outcomes in the targeted organs both *in vivo* and *in vitro* experiments must be carried out under controlled conditions (Andón et al. 2014; Arora et al. 2012).

In vitro assessment of nanoparticle toxicity has several advantages and some of these are: 1) revealing the effect of target cells in the absence of secondary effect due to inflammation, 2) the identification mechanisms that cause toxicity in the absence of compensatory and physiological factors present in whole animal studies 3) cost-effectiveness, rapidity, and efficiency, and 4) optimization of later whole animal studies based on the findings (Huang et al. 2010). Exclusively using *in vitro* tests increase the potential risks of not fully experiencing the pathogenic effects of coordinated tissue responses, toxicokinetics, and translocation reported in *in vivo* assessments. Certain cell toxicity assays, such as the neutral red, and MTT, have shown some limitations resulting in invalid test results due to adsorption and/or interaction of the dye products. Hence various assays should be performed on depending on the nanomaterial in question (Arora et al. 2012).

1.6.1 Nanotoxicity assessment

Several *in vitro* methods have shown to be reliable as an indicator to measure cell toxicity. These can be divided into cell viability assays that are comprised of (Takhar et al. 2011):

- Proliferative assays. E.g. tetrazolium salts assay (MTT, MTS), Alamar blue, [3H] thymidine, and cologenic.
- Apoptosis assays. E.g. DNA laddering, caspase, the comet, TUNEL, annexin V.
- Necrosis assays. E.g. neutral red uptake, trypan blue, LDH

In addition to the mentioned cell viability assays above we also have oxidative stress assays, and inflammatory assays. The MTT assay, a proliferative variant, is of interest to this project.

There are several advantages to *in vitro* test assays. Some that are worth being mentioned are: human cells (e.g. keratinocytes in the form of HaCaT cell in MTT) and tissues can be used, fast and cheap testing, small amount of the test material is required, controlled conditions, as well as a reduction of animal testing (Arora et al. 2012; Takhar et al. 2011).

1.6.2 MTT assay

Cytotoxic cell viability testing can be done based on several different methods such as counting dyed/non-dyed cells, assessing cell incorporation of radioactive nucleotides ([^{3}H] thymidine or [^{125}I] Iododeoxyuridine), and measuring the amount of ^{51}Cr-labeled protein after cell lysis. However, many of these methods are time-consuming and ill equipped to process huge numbers of samples. Conversely, an MTT assay is quantitative, rapid, and versatile (Mosmann 1983). The MTT assay has been used in different studies to evaluate the potential cytotoxic effects in nanomaterials such as silver NP, fullerenes, carbon NPs, and titanium oxide NPs (Arora et al. 2012).

MTT, 3-[4,5-dimethylthiazol-2-yl]-2,5-diphenyltetrazoliumbromide, $C_{18}H_{16}N_5SBr$, or thiazolyl blue tetrazolium bromide, is a yellow water-soluble dye that is absorbed by cells and reduced to formazan, ($C_{18}H_{16}N_5SBr$) by succinic dehydrogenase enzymes in active mitochondria (Figure 14).

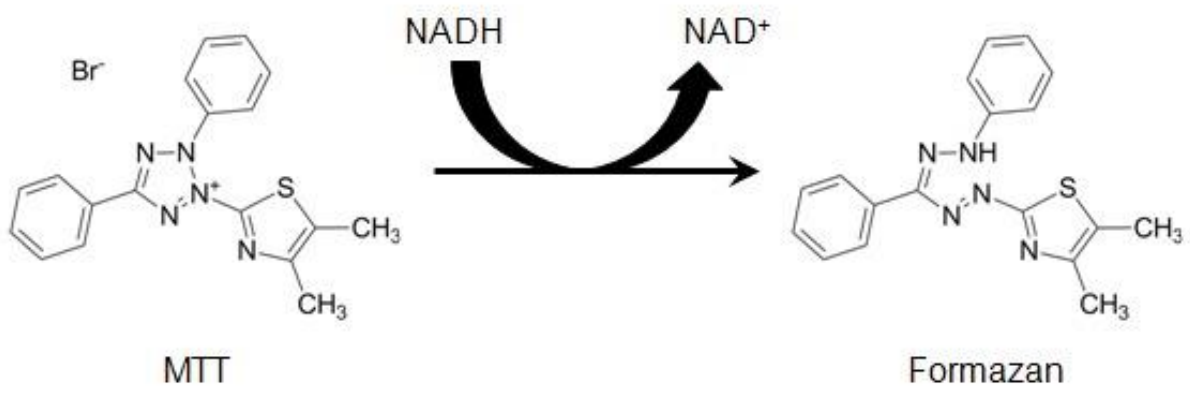

Figure 14: Reaction scheme for reduction of MTT to formazan (Sittampalam et al. 2004)(with permission)**.**

The amount of produced formazan is directly proportional to the number of living cells, as the conversion does not occur in dead cells; hence a lower concentration will indicate a certain degree of cytotoxicity when measured by optical density (Berridge et al. 1993; Borenfreund et al. 1988; Denizot et al. 1986; Mosmann 1983).

2 Aim

The general aim of this study was to optimize the NCE-containing nanoparticles for their NCE load and evaluate the system's toxicity.

The specific aims have been:

- Optimize the ratio of chitosan and lecithin in the nanoparticles with regard to their size, and NCE entrapment.
- Investigate NCE's toxicity through MTT assays conducted on HaCaT cells.

3 Materials and methods

3.1 Constituents

3.1.1 Materials

Acetic acid (≥99.8 %), Sigma-Aldrich, St. Louis, USA

Acetonitrile CHROMASOLV® gradient for HPLC (≥99.9 %), Sigma-Aldrich, St. Louis, USA

Ammonium acetate (98.0%), AnalaR NORMAPUR, VWR, Leuven, Belgium

ChitopharmTM S, Mw 50000 – 1000000 Da, approx. 85-90 % deacetylation, Chitinor AS, Haugesund, Norway

Dulbecco's Modified Eagle's Medium - high glucose, with 4500 mg/L glucose, L-glutamine, and sodium bicarbonate, without sodium pyruvate, liquid, sterile-filtered, suitable for cell culture. Sigma-Aldrich, St. Louis, USA

Dulbecco's Phosphate Buffered Saline modified, without calcium chloride and magnesium chloride, liquid, sterile-filtered, suitable for cell culture, Sigma-Aldrich, St. Louis, USA -

Ethanol (96 %, v/v), Sigma-Aldrich, St. Louis, USA

Hydrochloric acid

Isopropanol

Lipoid S45 (45 % (w/w) phosphatidylcholine), Lipoid GMBH, Ludwigshafen,

Germany Methanol, CHROMASOLV® for HPLC, Sigma-Aldrich, St. Louis, USA

MILLI-Q filtered water

New Chemical Entity, Photocure ASA, Oslo, Norway

RPMI-1640 Medium, with L-glutamine and sodium bicarbonate, liquid, sterile-filtered, suitable for cell culture, Sigma-Aldrich, St. Louis, USA

Thiazolyl Blue Tetrazolium Bromide, powder, BioReagent, suitable for cell culture, suitable for insect cell culture, ≥97.5% (HPLC), Sigma-Aldrich, St. Louis, USA

Triton X-100, for molecular biology, Merck KGaA, Darmstadt, Germany

Trypan Blue solution, 0.4%, liquid, sterile-filtered, suitable for cell culture, Sigma-Aldrich, St. Louis, USA

Trypsin-EDTA solution, 0.25%, sterile-filtered, BioReagent, suitable for cell culture, 2.5 g porcine trypsin and 0.2 g EDTA • 4Na per liter of Hanks′ Balanced Salt Solution with phenol red, Sigma-Aldrich, St. Louis, USA

3.1.2 Instruments

Aktilite® CL128, lamp for photodynamic therapy, Photocure ASA, Oslo, Norway

Holten Laminair, Holten safe 2000, model 1.2, Class II Laminar Air Flow Hood

IKA-colour squid white, magnetic stirrer, ID. No. 0003671000, Germany

Metrohm, 744 pH meter, type: 1.744.0010, Ion analysis, Metrohm, Herisau, Switzerland

MILLI-Q BIOCELL, 0.22 µm, Millipak® 40, Bergman AS, Trondheim, Norway

NICOMP Submicron particle sizer (PCS), model 370, NICOMP particle sizing system, Santa Barbara, USA

Sartorius BP211D, scale, Sartorius AG, Göttingen, Germany

Sartorius LP620S, scale, Sartorius AG, Göttingen, Germany

Waters e2795, HPLC separation module, Alliance HT, Waters Corporation, Milford, USA

Waters 2489, UV/visible detector for HPLC, Waters Corporation, Milford, USA Zetasizer nanoseries, model Zen 2600, Malvern Instrumentals Ltd, Malvern, UK

3.1.3 Software and programs

ELISA: SoftMax® Pro Software, version 5.4.1, Molecular Devices, 2010, Sunnyvale, USA

HPLC: Empower Pro, Empower 3 software, 2010, Waters Corporation, Milford, USA

PCS: CW388 Application version 1.68, NICOMP particle sizing system, Santa Barbara, USA

Zetasizer software 7.03, 2002-2013, Malvern Instrumental Ltd, Malvern, UK

3.1.4 Utensils

Accu-jet® pro Pipette Controller Brand, BrandTech Scientific, Wertheim, Germany

Acrodisc® 25 mm Syringe Filter with 0.2 µm Supor® Membrane, Sterile, Non-pyrogenic, Pall International, Fribourg, Switzerland

ART® 1000 E Barrier tip, Rached, Sterile, 1000 µL pipette tips, Thermo Scientific, Roskilde, Danmark

BD Plastipak™, 1 mL luer, Becton, Dickinson and Company, Franklin Lakes, USA BD Plastipak™, 2 mL luer, Becton, Dickinson and Company, Franklin Lakes, USA BD Plastipak™, 5 mL luer, Becton, Dickinson and Company, Franklin Lakes, USA BD Plastipak™, 10 mL luer, Becton, Dickinson and Company, Franklin Lakes, USA

Corning® 4870 Costar® reagent reservoirs, capacity 50 mL, white polystyrene

Dialysis membrane, Visking, Size 1, Inf. Dia. 8/32”, 6.3 mm: 30 M (approx.), Medicell Membranes Ltd., London, UK

Disposable cuvettes, standard, Brand®, Wertheim, Germany

Falcon® Serological pipette, sterile-R, non-pyrogenic, 5 mL, Corning incorporation, Life sciences, One bection circle, Durham, USA
Falcon® Serological pipette, sterile-R, non-pyrogenic, 10 mL, Corning incorporation, Life sciences, One bection circle, Durham, USA
Falcon® Serological pipette, sterile-R, non-pyrogenic, 25 mL, Corning incorporation, Life sciences, One bection circle, Durham, USA
Finnpipette®, 200-1000 µL, Thermo labsystems, Helsinki, Finland Finnpipette® F2, 20-200 µL, Thermo scientific, Vantaa, Finland Finnpipette® F2, 0.5-5 mL, Thermo scientific, Vantaa, Finland
Nunc® EasYFlasks™, Nunclon® Delta Surface, 25 cm^2 angled neck, filter cap, Thermo Fisher Scientific, Roskilde, Denmark
Nunc® EasYFlasks™, Nunclon® Delta Surface, 75 cm^2 angled neck, filter cap, Thermo Fisher Scientific, Roskilde, Denmark
Nunc® EasYFlasks™, Nunclon® Delta Surface, 175 cm^2 angled neck, filter cap, Thermo Fisher Scientific, Roskilde, Denmark

Waters Atlantis T3 4.6 x 150 mm HPLC-column, Milford, USA
Waters Atlantis T3 5 µm, 4.6 x 20 mm guard cartridge, Milford, USA

3.1.5 Biological material
HaCaT cells passages 62-71
Fetal bovine serum

3.2 Preparation and characterization of nanoparticles

3.2.1 Preparation of empty NPs
This method was based upon a modified method developed by Hemmingsen (Hemmingsen 2015; Sonvico et al. 2006)
The nanoparticles were prepared by adding 0.5 mL of a chitosan solution in acetic acid (0.5 %, w/v) to 44 mL milli-Q water. Four mL of the ethanolic lecithin solution (2.5 %, w/v) was slowly injected to the chitosan solution in milli-Q water through a syringe (2.00 mL/min) under mechanical stirring at 450 rpm. The ratio of chitosan and lecithin was 1:20 (w/w). The suspension was stirred for approximately 1 hour and left in the refrigerator overnight before further investigation.

3.2.2 Preparation of NCE-containing NPs

This method was based upon a modified method developed by Hemmingsen (Hemmingsen 2015; Sonvico et al. 2006)

The nanoparticles were prepared by adding 1.00 mL, 0.5 mL, or 0.25mL of a chitosan solution in acetic acid (1 %, w/v) to 44 mL milli-Q water. NCE (50, 75, or 100 mg) was dissolved in 4 mL of the ethanolic lecithin solution (2.5 %, w/v) injected to the chitosan solution in milli-Q water through a syringe (2.00 mL/min) under mechanical stirring at 450 rpm. The ratio of chitosan and lecithin was 1:10, 1:20, and 1:40 (w/w). The suspension was stirred for approximately 1 hour and left in the refrigerator overnight before further investigation.

3.2.3 Analysis of particle size

This method was based upon a modified method developed by Hemmingsen (Hemmingsen 2015)

The size of the nanoparticles was determined by photo correlation spectroscopy (PCS) on the NICOMP Submicron particle sizer, model 370, with an angle of 90 degrees. The temperature of the measurements was 24°C ± 1°C. The samples of particle suspensions were prepared in a laminar airflow (LAF) bench to provide a particle-free preparation environment. Due to this, the measuring tubes were sonicated for 60 minutes in milli-Q water, and rinsed 3 times with filtered water (0.2μM pore size) before each measurement. The samples were diluted with filtered water to attain an intensity of 250-370 KHz throughout of the measurements. The size distribution of the NPs in suspension measured in 4 cycles of 10 minutes.

3.2.4 HPLC analysis

This method was based upon a modified method developed by Hemmingsen (Hemmingsen 2015)

The preparation of the mobile phases and dilution solvent was based on a method developed by Photocure ASA. Two mobile phases, namely mobile phase A and B were prepared by dissolving 1.5 g ammonium acetate in acetonitrile and water (volume ratio of 100:900 mL; A and 900:200 mL; B (v/v)). To prepare a calibration curve, six standard solutions (2 1.5, 1, 0.75, 0.5 and 0.25 mg/mL) were prepared from a stock solution (10 mg/mL) by diluting with a dilution solvent. The dilution solvent was prepared by mixing 40 mL of the mobile phase A with 160 mL of mobile phase B. The HPLC analysis was carried out by using an Atlantis T3 4.6 x 150 mm column, and an Atlantis T3 5 μm 4.6 x 20 mm guard cartridge.

44

The conditions for the HPLC analysis are described in Table 1. The conditions for the shutdown method are described in Table 2. Both of these methods were mostly as described in Hemmingsen (Hemmingsen 2015) to ensure a similar results.

Table 1: Conditions of the HPLC analysis

Conditions for the HPLC analysis	
Flow	0.4 mL/min
Column temperature	25 ± 5 °C
Sample temperature	25 ± 5 °C
Wavelength of the detector	270nm
Solvents	Solvent A: Mobile phase A
	Solvent B: Mobile phase B
Run time	Run time
Equilibration time	3 minutes
Gradient	0 % mobile phase A to 19.8 % mobile phase A

Table 2: Conditions for the shutdown method

Conditions for the shutdown method	
Flow	1 mL/min
Column temperature	Column temperature 25 ± 5 °C
Sample temperature	Sample temperature 25 ± 5 °C
Wavelength of the detector	Wavelength of the detector 270 nm
Solvent	Solvent C: Acetonitrile

3.2.5 Preparation of samples for HPLC analysis and evaluation of NCE entrapment

This method was based upon the method developed by Hemmingsen (Hemmingsen 2015). The determination of the entrapment efficiency was done by dialysis followed by the HPLC analysis. The NCE-containing NPs were separated from unentrapped NCE by dialysis in dialysing tubing. 20 mL of the samples were dialysed against 500 mL milli-Q water for 6 hours. An aliquot (500 µL) of the NCE-containing NPs free from unentrapped NCE was dissolved in 500 µL methanol to destroy the NPs. This solution was analysed using the same HPLC method as described above. The amount of free (unentrapped) NCE in dialysis medium was also determined by HPLC analysis. To determine the recovery, a sample (500 µL) of the original NCE-containing NPs suspension (containing both free and entrapped NCE) was dissolved in 500 µL methanol to destroy the NPs and analysed using HPLC. All measurements were performed in triplicates.

3.2.6 Zeta potential

Zeta potential was measured using Zetasizer Nano Z 2600. Before each measurement the cells were rinsed 2 times with ethanol and 3 times with milli-Q water using a 1 mL syringe. 75 μL of the samples were diluted with milli-Q water to the total volume of 1 mL, before being transferred to the measurement cell. Each sample were run 3 times at 25°C.

3.2.7 Determination of pH

The measurement of the pH of the samples was done with Metrohm, 744 pH meter at room temperature (25±1°C) for all the NPs suspensions.

3.2.8 Toxicity testing

3.2.8.1 Cell Splitting

The HaCaT cells were split at around 60-80% confluence.

The Modified Eagle's Medium, the Phosphate Buffered Saline as well as the Trypsin-EDTA was heated to 37 °C cabinet for 1 hour. The LAF bench, and all equipment were cleaned with 70% ethanol before entry to ensure sterile conditions. For the 25F, 75F and 175F culture bottles 5, 15, or 25 mL of PBS was added respectively and then aspirated from the bottle.

Trypsin-EDTA solution (1, 2, or 3mL) was then added to the 25F, 75F and 175F bottles respectively. The bottles were tilted to mix and ensure that the entire surface was covered before aspiration. The cell culture bottles were then incubated at 1-3 minutes or until cell detachment.

MEM (5, 15 or 25 mL) was added to respectively 25F, 75F and 175F flasks to stop the trypsinization. An appropriate volume of the cell suspension was then added to each new bottle in order to make a certain ratio (e.g. 5 mL).

3.2.8.2 MTT Assay

The cell culture bottles were prepared in the same way as the splitting in **3.2.8.1** for cell detachment purposes, although RPMI was used instead of MEM for trypsin inhibition. A small sample at around 10 μL was taken from one of the flasks and applied to hemocytometer

with a cover glass atop. Trypsin blue dye was deemed unnecessary in our case since cell viability was readily established.
The following equation was used in order to calculate the amount of cells per mL in the medium:

$$a = (\frac{(z+y+x)}{3} \cdot 10000)$$

Where *a,* represents the amount of cells per mL, and *z, y, and x* represents the cells counted in 3 different grids. Following, the total amount of cells present were calculated by this formula:

$$Cells_{total} = a \cdot b$$

Where *a,* denotes the amount of cells per mL, and *b* denotes the total volume of the medium.

The remaining cells were re-suspended with RPMI transferred to a 50 mL Falcon tube, and centrifuged at 1500rpm(2,5) for 6 minutes. The supernatant was mostly aspirated; leaving a small covering layer of RPMI ensuring the pellet remained untouched. RPMI, *x*. 1 mL of warm MEM+FBS was added to the pellet before re-suspension. This amount was regarded as concentrated cell solution (CCS).

For a 96-well plate a minimum of 2 x 10^6 cells were required to be suspended in a 10 mL solution of RPMI, which includes the CCS. The cells were then seeded; 100 µL of cell suspension per well and left over night in the cell incubator.

Two parallel assays were performed. The first had 8 dilution series: 50, 100, 150, 200, 250, 300, 400, 500 µg/mL by dissolving 100mg of NCE in RPMI. The second parallel was performed by using the 1:20 ratio of empty NPs and NCE containing NPs. The dilution series were as based on using a certain amount of the NP solution: 100, 200, 300, 400, 500, 600, 800, 1000 µL.

In both parallels Triton served as a positive control, while RPMI as a negative control. Hundred µL of each of the controls were added to their respective wells. The Triton solution was made by using 20 µL Triton in 980 µL RPMI. After 4 hours of incubation 10 µL of MTT

solution (5 mg MTT per mL PBS) was added to every well and mixed. This was followed by 2 additional hours of incubation.

A volume of 70 µL was carefully removed from all of the wells while avoiding touching the bottom of the well with the tip of the pipette. 5 mL of acid propanol (0.04 M HCl in isopropanol) was then added to the multichannel plate, and 100 µL was added to all the wells. The wells were re-suspended by pipetting until a "squish" noise occurred. The plate was then put in the orbit shaker for 1 hour at room temperature.

The absorbance was then measured at 590 nm on a microtitre plate reader, or an ELISA test as it is also called. Cell survival was determined from the absorbance value in comparison to the negative control and the positive control.

3.2.9 Statistical Analysis

Statistical data was analysed by performing Student's t-test. The confidence level used in the calculations was 95 % for all the measurements, and $p<0.05$ as minimal level for significance.

4 Results and discussion

4.1 Nanoparticle characterization

The size and the polydispersity index of all of the nanoparticles (empty and NCE-containing NPs) were determined by previously described method (section **3.2.3**), and are presented in Table 3 as a NICOMP distribution. The NICOMP size distribution bimodally (two peaks) arranges the particles in population groups based on their size, and are presented as a percentage with a specific mean diameter (Andersen et al. 2013). In this experiment the NICOMP distribution generally showed three populations. The majority were lower than the mean size value in the table below ranging from 1 to 30 in presented percentage, there were however also some populations above the means size value that presented in the percentage range of 3 to 59. The high percentage could represent both particle aggregation as well as large NPs, and may have been due to the samples not being measured as freshly as possible.

The residual values were 11.1 ± 2.9 (1:10, n=9), 9.3 ± 2.3 (1:20, n=9), and 8.0 ± 2.0 (1:40, n=9) for the NCE-containing NPs, and 22.3 ± 17.9 (1:20, n=3) for the empty NPs. The values denote detected aggregates worth discarding in the sample, and should be as low as possible and optimally zero (Frantzen et al. 2003). The results findings were acceptable and significantly lower than in the project by Hemmingsen *et al.* (Hemmingsen 2015). Hence, the large NP size was likely not due to aggregation.

A substantial amount of nanoparticle mean sizes were larger than both the aimed value and the expected value at 200 to 300 nm (Hurler et al. 2012; Sonvico et al. 2006). In the original study using the same CLNPs as in this project, and a CL ratio of 1:5 to 1:80, particle aggregation was quite evident at 1:40 ratio, while 1:5 through 1:20 showed a stable colloidal suspension, a mean size below 280 nm and a polydispersity index (PI) below 0.2 (Sonvico et al. 2006). In the thesis from last year the CLNPs were evaluate with the ratios 1:5 to 1:20, and found to be larger than the size in previously mentioned study. The size range varied from 1089 to 318 nm, and decreased in value as the lecithin amount was increased with regards to the ratio. In a study by Şenyiğit *et al.* using the same CLNPs loaded with clobatasol-17-propionate, and 1:20 ratio; the mean size was 248.25 ± 15.13 nm (Şenyiğit et al. 2010). Tan *et al.* performed a study on the 1:20 ratio CLNPs loaded with quercetin and found a mean size of 168.0 nm substantially lower than our findings (Tan et al. 2011). Özcan *et al.* did a study

with 1:20 ratio CLNPs that resulted in a size of 274.6 ± 14 nm; smaller than the mean found in our project (Özcan et al. 2013).

The polydispersity index is a description of the width of the overall distribution given a single mean. A High PI value represents a wide distribution while low PI values, which is opted, represent a narrow size distribution.

Table 3: Characteristics of empty CLNPs and NCE-containing CLNPs (mean ± SD, n=3)

pH	C/L ratio	Amount NCE (mg)	Size (nm)	PI	ZP (mV)	EE%	RR%
4.88	1:20	0*	54.4±40.2	0.416±0.071	23.1±0.469	-*	-*
4.24	1:10	50	486.3±197.9	0.295±0.033	59.3±0.571	81.70±0.30	103.60±2.45
3.82	1:10	75	373.2±207.4	0.280±0.024	59.9±0.745	59.03±0.23	82.80±1.25
3.76	1:10	100	364.7±120.9	0.353±0.034	66.3±1.15	44.30±0.10	77.27±0.78
3.91	1:20	50	365.5±173.8	0.263±0.077	32.4±0.825	80.77±1.03	101.27±0.76
3.79	1:20	75	244.4±123.5	0.272±0.028	42.1±0.888	55.70±2.61	98.10±0.40
3.64	1:20	100	333.9±149.5	0.267±0.018	40.4±0.947	42.07±0.32	76.33±1.07
3.82	1:40	50	173.9±69.2	0.229±0.017	16.5±1.67	84.4±0.17	111.77±0.57
3.74	1:40	75	351.4±67.9	0.268±0.028	42.0±0.926	58.33±6.28	100.20±1.42
3.63	1:40	100	208.0±78.5	0.296±0.067	24.2±0.806	42.87±0.06	72.37±0.35

*The first row denotes the empty CLNPs, thus no value is available for EE%, and RR%.

The suspensions also displayed a quite high PI for the empty NP, and a relatively high PI for the NCE-containing NPs (Hemmingsen 2015). In another study using the colloidal suspension and a 1:10 and 1:20 CL ratio, the same inverse relationship was seen between the size and the amount of lecithin, and the polydispersity index was also relatively high (Hafner et al. 2011). In another study the PI was found to be rather low at 0.110 ± 0.01 (Şenyiğit et al. 2010). The results from our experiments showed the same trend in decreasing mean NP size as the

lecithin was increased, a higher PI for the empty NPs compared to the loaded NPs, a relatively high but acceptable PI for the NCE-containing NPs, as well as a mean size that was larger than the original study. The study by Tan *et al* showed a relatively high polydispersity index at 0.331, which is comparable to our values (Tan et al. 2011). The PI value in the study with Özcan *et al.* at 0.241 ± 0.02 was lower than the values found in our project (Özcan et al. 2013).

The zeta potential describes the electrostatic potential of the double layer surrounding a NP in a solution. NPs with ZP in range of -10 to +10 mV are considered neutral, while ZP values less than -30 and greater than +30 mV are respectively considered to be strongly anionic or cationic. ZP affects suspension stability, and either strongly cationic or anionic suspensions tend to have greater stability due to electrostatic repulsion, which prevent particle aggregation. ZP may also be used to evaluate if drugs are adsorbed onto the surface or encapsulated. Due to the fact that most cell membranes are cationic ZP may affect permeation, and cationic particles usually displaying toxic effect by rupturing the cell wall (Clogston et al. 2011; Mohanraj et al. 2007).

The zeta potential values in Table 3 were rather high and appeared to increase after the NPs contained NCE (32.4 ± 0.825 to 42.1 ± 0.888 mV). This suggested that a portion of the NCE might have been adsorbed onto the surface of the NPs, seeing that the empty NPs, caused by the protonation of chitosan in low pH, did not have the same extent of surface charge. The low pH might additionally have pronated the NCE. As the CL ratio was changed in favour for lecithin, the same trend in ZP was observed in our results as was present in previous studies (Hafner et al. 2011; Hemmingsen 2015; Sonvico et al. 2006). This is thought to be due to the decreasing amount of chitosan present in the NP. In the study performed by Şenyiğit *et al.* the ZP for the 1:20 ratio was found to be 34.10 ± 1.80 mV, a bit lower than two of our values, and slightly higher than one (Şenyiğit et al. 2010). A ZP of 10.85 ± 0.05 mV was found for the drug loaded NPs in a study done by Tan *et al*. a value considerably lower than the ones found in our project (Tan et al. 2011). The study with Özcan *et al.* showed the ZP to be 40.8 ± 2.80 mV, which is similar to our discovered values (Özcan et al. 2013).

4.2 HPLC analysis

The entrapment efficiency and relative recovery of the NCE-containing NPs was assessed by a HPLC analysis method developed by Photocure ASA, and modified by in the project preceding this one (Hemmingsen 2015). The entrapment efficiency was determined by dialysis. The same reverse-phase C_{18} column and mobile phases were used in this project as the previous projects (Hadafow 2014; Hemmingsen 2015). Hemmingsen developed and validated the run conditions for the HPLC by using a single NCE concentration (5 mg/mL), and a slow gradient change of the mobile phase before calculating the mobile phases' ratio based on peak appearance on the chromatogram. A standard curve (Figure 15**)** for the NCE was prepared based on these settings.

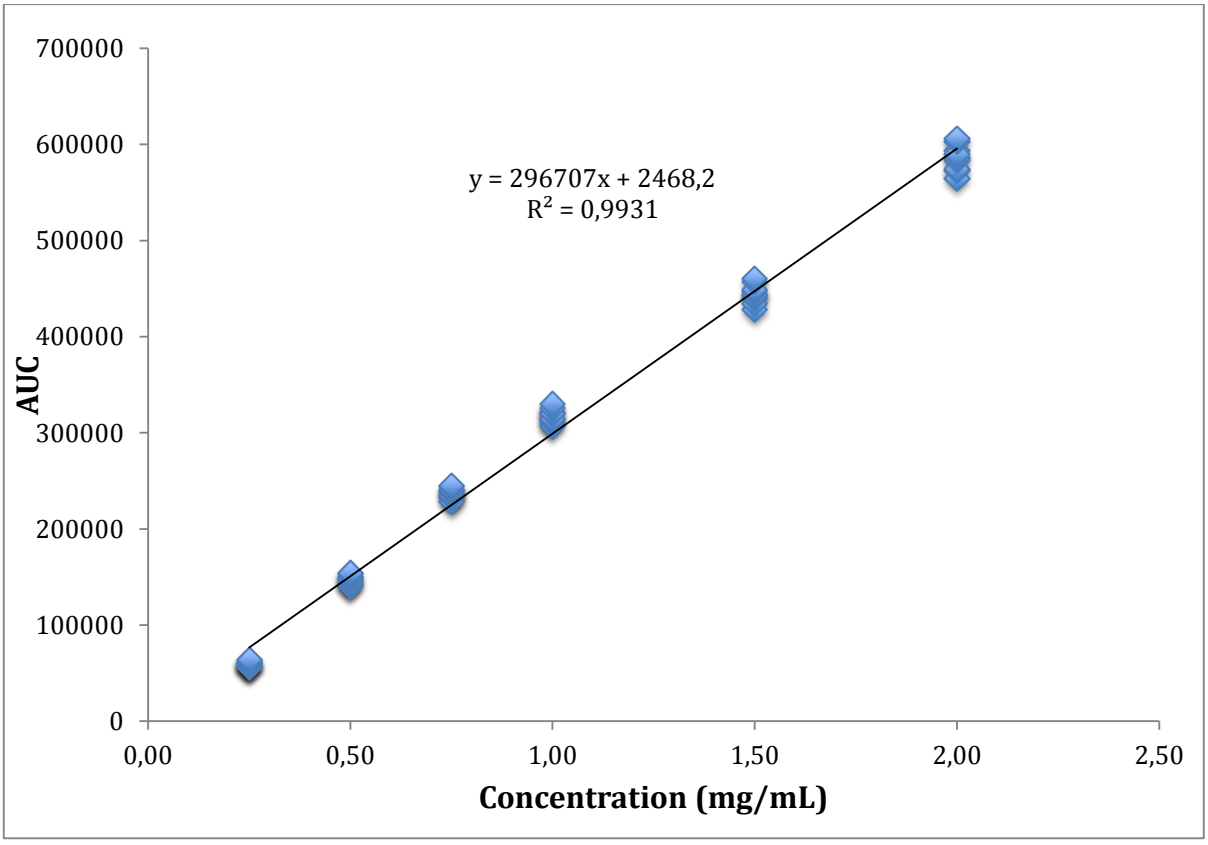

Figure 15: Standard curve for the NCE based on the concentration 0.25, 0.5, 0.75, 1.0, 1.5, and 2.0 mg/mL (n=3).

The standard curve was used to quantify the amount of NCE present in the different undetermined CLNP samples. The standard curve is in this project is comparable Hemmingsen's (R^2=0.9977), but had a lower R^2 value despite of repeated attempt to improve the curve (Hemmingsen 2015). The same challenges were faced during this project, mainly the deviations due to the rapid degradation of NCE by hydrolysis, which likely affected the readings. A similar separation as Hemmingsen's was also seen concerning the main NCE peak and degradation product (Figure 16).

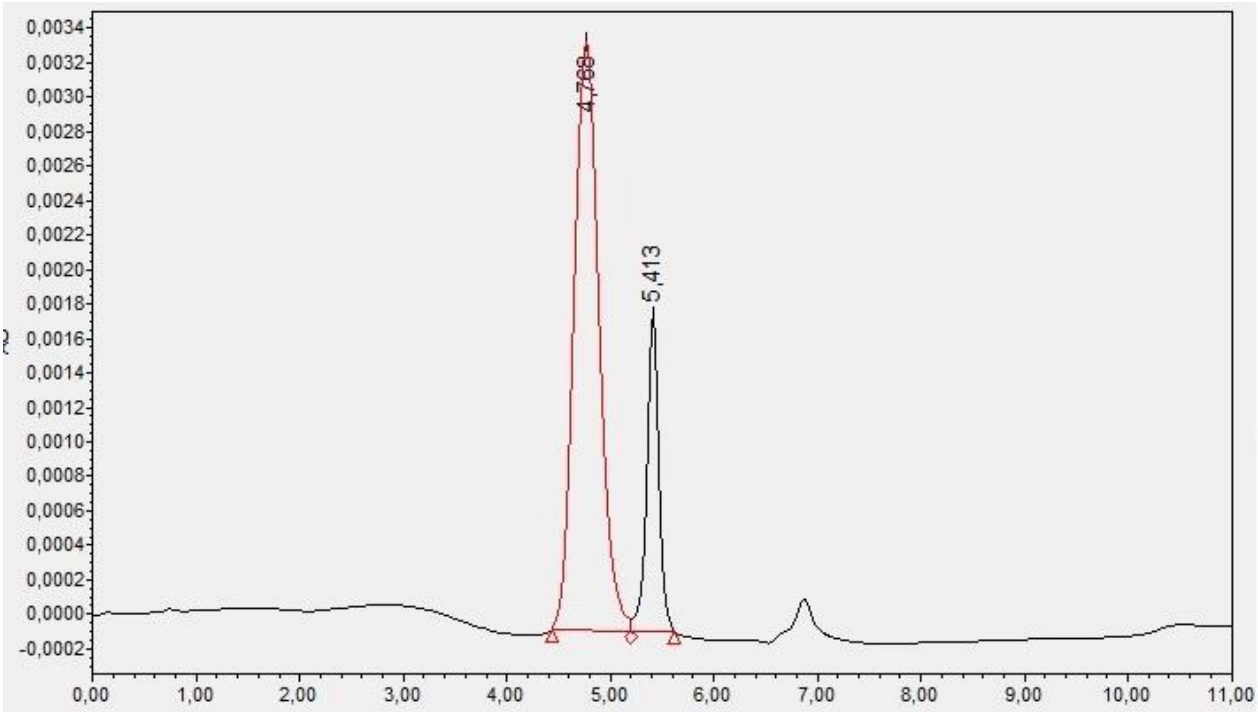

Figure 16 HPLC chromatogram for 0.25 mg/mL NCE. The NCE is the peak at 4.768 and the first degradation product at 5.413. The second degradation product is slightly visible at around 7.

The entrapment efficiency presented in Table 3 was found to be satisfactory ranging between 42.9 to 84.4% being highest in all of the NPs loaded with 50 mg NCE; this is in contrast to the findings of both Hemmingsen (11.60 ± 2.13%) and Thoresen (23 ± 0.2%) (Hemmingsen 2015; Thoresen 2014). However it is in similarity although higher, 18.2 to 57.2%, to the study performed by Sonvico *et al.* showing the encapsulation efficiency of hydrophobic drugs such as progesterone are suited for CLNPs (Sonvico et al. 2006). In the study by Şenyiğit *et al.* the EE was even high than in our case 92.2 ± 0.5%, this was however due to the presence of isopropyl myristate (permeation enhancer) (Şenyiğit et al. 2010).

4.3 Toxicity assay

5-ALA has shown promise as an antimicrobial PDT agent, however it is essential that toxic effects are not exerted on healthy skin cells as this has not been investigated thoroughly (Harris et al. 2012). Chitosan and lecithin have proved to be non-toxic, as well as showing little to no irritation (Dash et al. 2011; Elnaggar et al. 2014; Paolino et al. 2002). The same chitosan/lecithin (CL) NPs as in this project have also proven to be non-toxic, however 5-ALA-in-CL-NPs have yet to be investigated with regards to skin cell toxicity (Hafner et al. 2011). In this project, we investigated the toxicity of 5-ALA as a free drug, as well encapsulated in CLNPs on HaCaT cells in varying concentrations.

The following equation was used to calculate the cell viability percentages (Lai et al. 2012):

$$(viable\ cell\ \%) = \left(\frac{OD\ of\ drug\ treated\ sample}{OD\ of\ untreated\ sample}\right) \times 100$$

Experiment 1

In the first experiment we focused on testing the toxicity of the free drug towards the HaCaT cells in the following concentrations 50, 100, 150, 200, 250, 300, 400, and 500 mg/mL.

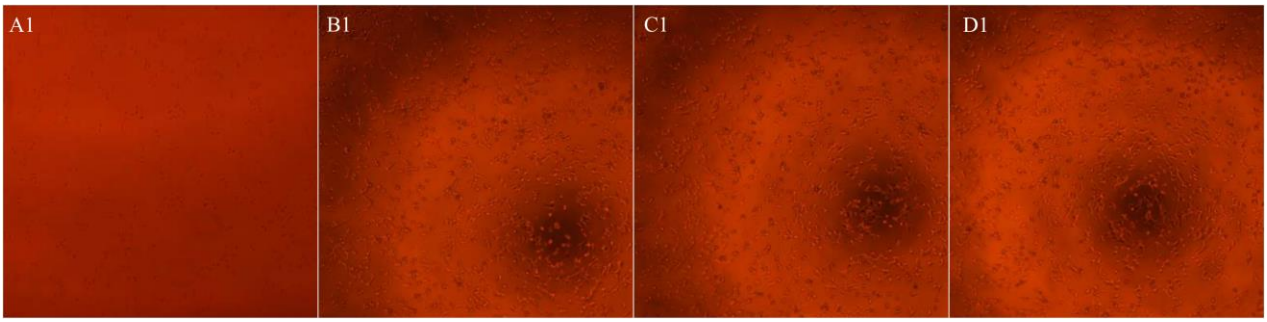

Figure 17: Micrographs of the HaCaT cells the first MTT experiment. Respectively A1 to D1 represents the wells with triton, 150 mg/ml NCE, 400 mg/ml NCE, and RPMI.

The micrographs **(**Figure 17) shows the viable HaCaT cells after 4 hours of incubation but before the MTT was added, thus suggest that the free NCE does not seem to produce any cytotoxic effect.

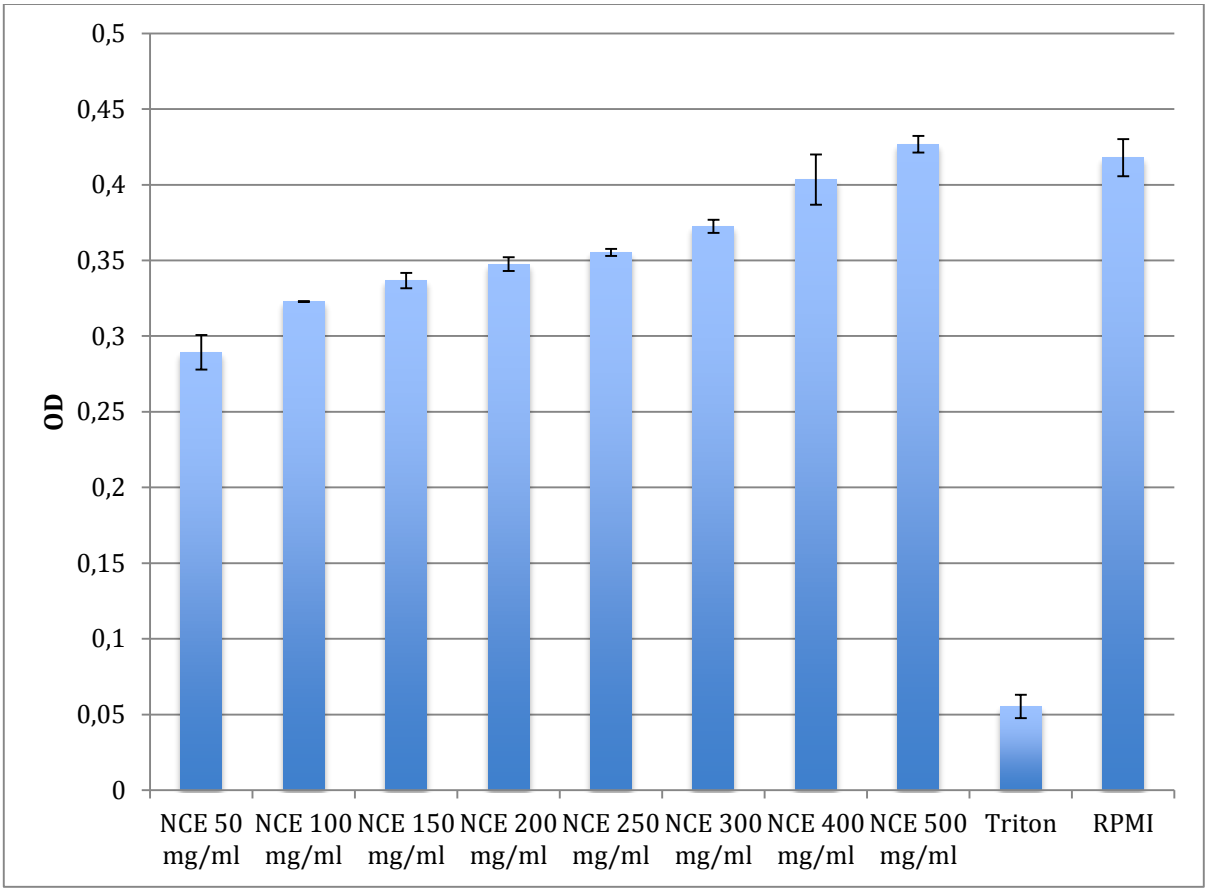

Figure 18: Column graph representing the OD for free NCE from experiment 1 (mean ± SD, n=3 for NCE).

After the MTT was added we were able to use the ELISA reader to do a quantitative analysis with regards to the cell toxicity. The results are the average from three replicates. The absorbance values (Figure 18) suggested that cell toxicity towards the free drug was inversely proportional to the NCE concentration. That is, the higher the NCE concentration; the lower the cell toxicity. Thus NCE seemed to have little to no toxic effect on HaCaT cells.

The cytotoxic profile for free NCE is presented in Table 4 as percentage of surviving cells. The concentration range 50-300 mg/mL showed a slight decrease in cell viability, but this was found to be insignificant ($p > 0.05$), while the 400 mg/mL concentration had an increase in viability, this difference was also found to be insignificant ($p > 0.05$). The previously suggested inverse proportionality between the toxicity and the concentration was first observable in in the 500 mg/mL concentration ($p < 0.05$).

Table 4: Cell viability of HaCaT cells towards free NCE in experiment 1 (mean ± SD, n=3).

Free [NCE] (μg/mL)	Surviving cells %
50	88.0±14.2
100	92.5±13.2
150	92.9±9.7
200	94.7±11.2
250	95.3±9.3
300	96.8±7.5
400	100.4±6.7
500	101.1±0.5

Experiment 2 and 3

In the second experiment we continued our toxicity testing, this time focused on potential synergistic effect of encapsulating NCE in the NPs, as well as the toxicity for the empty NPs. The following concentrations of NPs-containing NCE were tested: 103.1, 206.2, 309.3, 412.4, 515.5, 618.6, 721.7, and 824.8 μg/mL. Whereas empty CL NPs concentrations for chitosan where in the following range: 10.31, 20.62, 30.93, 41.24, 51.55, 61.86, 77.22, and 82.47 μg/mL, and the corresponding values for lecithin were respectively 206.2, 412.4, 618.5, 824.8, 1031.0, 1237.2, 1544.4, and 1649.4 μg/mL. Both of the NPs had a chitosan: lecithin ratio of 1:20.

Experiment 2

The OD_{590} results from experiment 2 are presented as a column graph in Figure 19, showing the different concentrations of both the empty and the NCE-containing NPs, triton (positive control - no cells)) and RMPI (negative control – untreated cells).

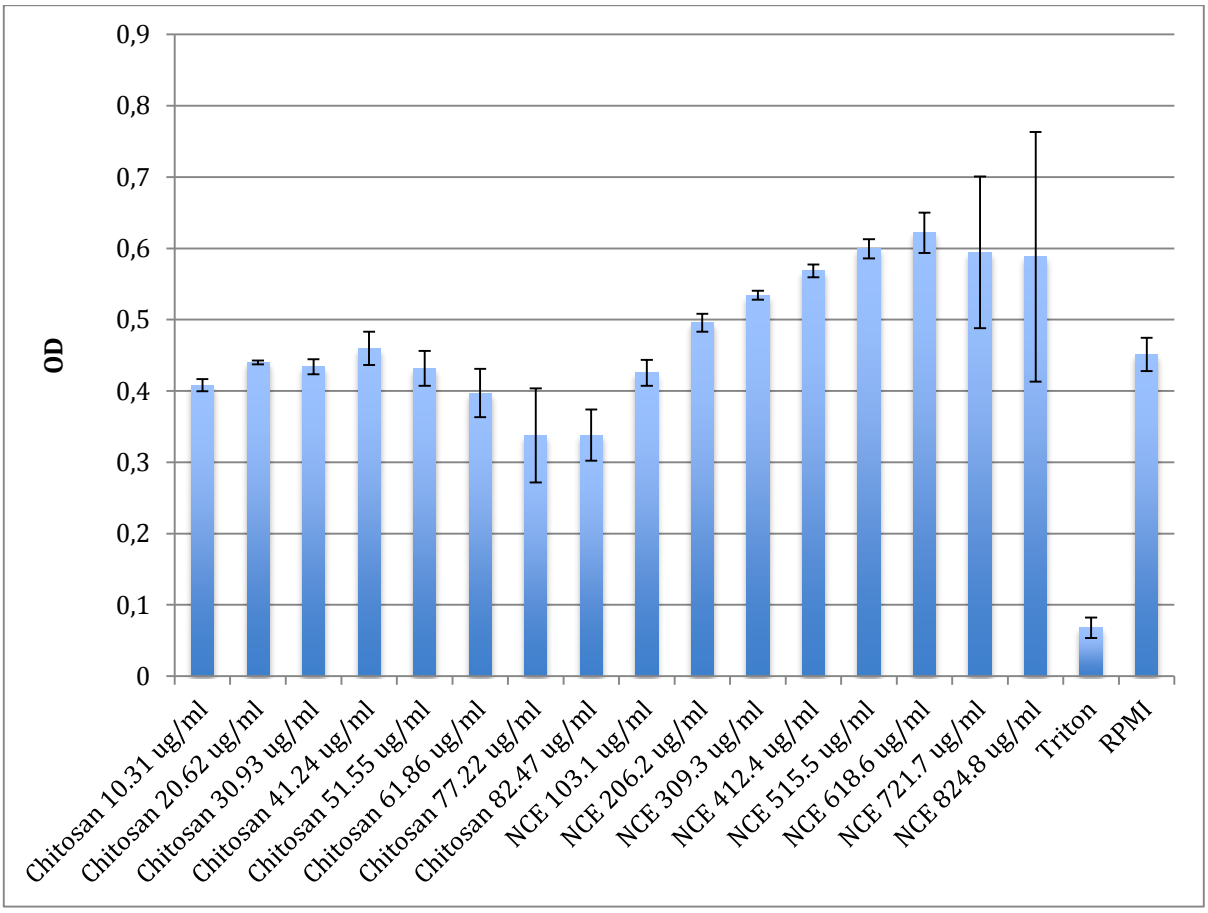

Figure 19: Column graph representing the OD from experiment 2 (mean ± SD, n=3). Chitosan denotes the empty chitosan NPs, while NCE is the CLNPs containing NCE.

The cytotoxic profile for empty NPs and NCE-containing NP is presented in Table 5 as percentage of surviving cells. The two lowest concentrations of empty NPs produced a decrease in cell viability ($p < 0.05$), while the rest of the concentrations were found to be insignificant ($p > 0.05$). These results are similar to the findings in a study where lecithin concentrations in the range of 50-400 µg/mL, in 1:20 ratio CL NPs, were evaluated and found to have no adverse effect on metabolic activity or cell viability towards both fibroblasts and HaCaT cells. However, after increasing the incubation time from 2 hours to 24 hours the authors found significant reductions in the cells metabolic activity for lecithin concentrations of 200 µg/mL and upwards (Hafner et al. 2011). The decrease in percentage of surviving cells in the lowest NCE-containing NP concentrations, as well as the increase in the two highest

concentrations were found to be insignificant ($p > 0.05$), while the rest of the remaining results were considered to be significant ($p < 0.01$).

In addition to this, the same proportional relationship between the cell viability and NCE concentration seemed to be present as earlier observed with the free NCE. That is, as CL concentration increases the higher the percentage of cell survival.

Table 5: Cell viability of HaCaT cells towards chitosan/lecithin concentration in empty NPs and NCE-containing NPs in experiment 2 (mean ± SD, n=3).

[C/L] in empty NPs (µg/mL)	Surviving cells (%)	[NCE] in NPs (µg/mL)	Surviving cells %
10.31/206.2	83.0±5.6	103.1	94.3±4.0
20.62/412.4	94.2±2.8	206.2	109.8±2.8
30.93/618.5	94.6±4.3	309.3	118.4±1.4
41.24/824.8	97.6±3.7	412.4	126.0±2.0
51.55/1031.0	102.0±13.0	515.5	132.8±3.0
61.86/1237.2	102.3±9.9	618.6	137.8±6.3
77.22/1544.4	104.2±19.7	721.7	131.8±23.6
82.47/1649.4	98.3±16.3	824.8	130.4±38.8

Figure 20 clearly shows the viable HaCaT cells before MTT addition (B1 to D1), and the formazan stain in B2 to D2 shows the persisting metabolic activity of the cells. In A1 and A2 on the other we can observe that triton exerted its cytotoxic effect and no cells are present.

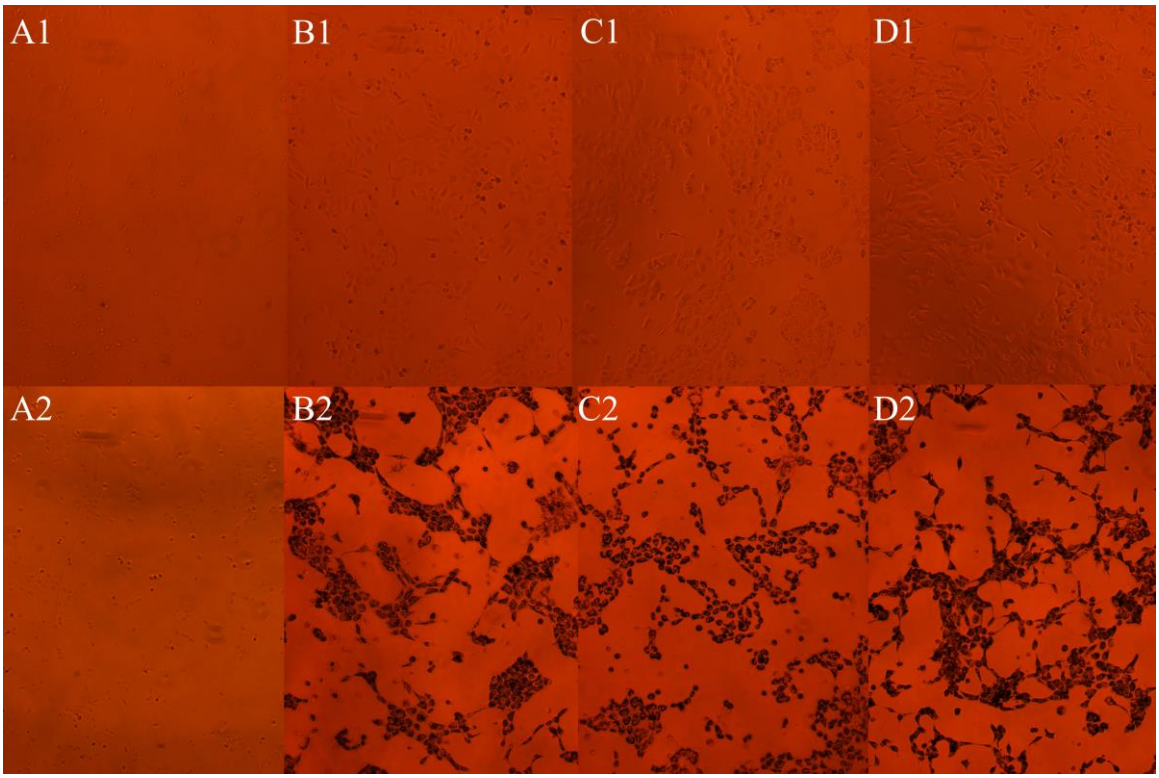

Figure 20: Micrograph of the second MTT experiment. Respectively A to D denotes triton, empty NPs, and NCE-containing NPs. The number 1 denotes before MTT addition, while 2 is after.

Experiment 3

The results presented in Figure 21 show a similar OD_{590} results as we observed in experiment 2's Figure 19, with the exception to overall higher values for the NCE-containing NPs as well as a lower RPMI value.

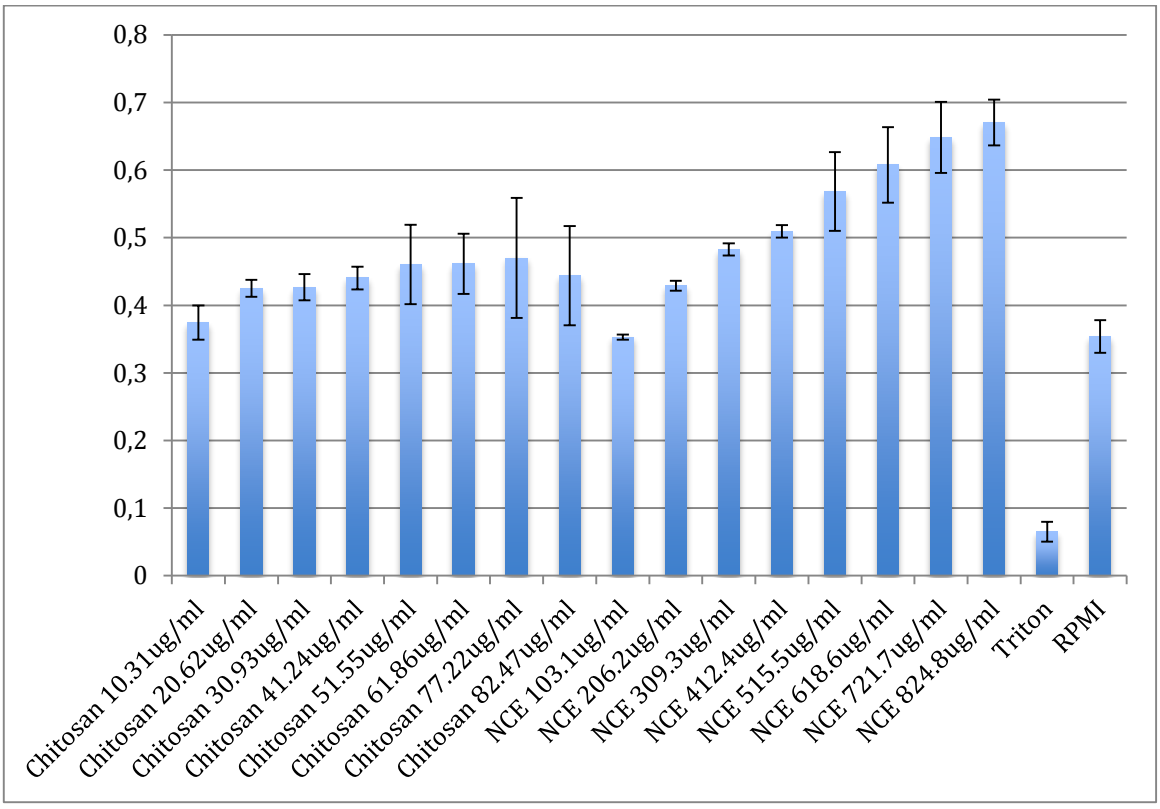

Figure 21 Column graph representing the OD from experiment 3 (mean ± SD, n=3). Chitosan denotes the empty chitosan NPs, while NCE is the CLNPs containing NCE

The second cytotoxic profile for empty NPs and NCE-containing NP is presented in Table 6 as percentage of surviving cells. No toxicity was found towards the empty NPs with regards to the all chitosan/lecithin concentrations, and except from the lowest CL concentration ($p > 0.05$), the results showed a significant increase in cell viability ($p < 0.01$). These results are dissimilar to the findings in the previously mentioned study (Hafner et al. 2011); this could be due to the low OD absorbance of RPMI, which results in a higher surviving cells percentage. The decrease in cell viability in the lowest concentration of NCE-containing NPs was found to be insignificant ($p > 0.05$), whereas the other concentrations where found to be significant with regards to increased cell viability ($p < 0.001$). The proportional relationship between NCE concentration and cell viability seems to also be present in this experiment.

Table 6: Cell viability of HaCaT cells towards chitosan/lecithin concentration in empty NPs and NCE-containing NPs in experiment 3 (mean ± SD, n=3).

[C/L] in empty NPs (µg/mL)	Surviving cells (%)	[NCE] in NPs (µg/mL)	Surviving cells %
10.31/206.2	105.8±7.2	103.1	99.7±1.1
20.62/412.4	120.1±3.5	206.2	121.2±2.1
30.93/618.5	120.6±5.5	309.3	136.4±2.5
41.24/824.8	124.4±4.8	412.4	143.9±2.6
51.55/1031.0	130.1±16.5	515.5	160.6±16.4
61.86/1237.2	130.4±12.6	618.6	171.7±15.8
77.22/1544.4	132.8±25.1	721.7	183.1±14.8
82.47/1649.4	125.4±20.7	824.8	189.4±9.6

Figure 22 shows similar results as observed in Figure 20; viable HaCaT cells before MTT addition (B1 to D1), and the formazan stain (B2 to D2) shows the persisting metabolic activity of the cells. In A1 and A2 on the other we can observe that triton exerted its cytotoxic effect and no cells are present. Most studies concerning cytotoxicity of chitosan were carried out over 4 hours as in our project, which does not completely enable the assessment of cellular responses caused prolonged or repetitive chitosan exposure; an important aspect of chronic therapy (Loh et al. 2012).

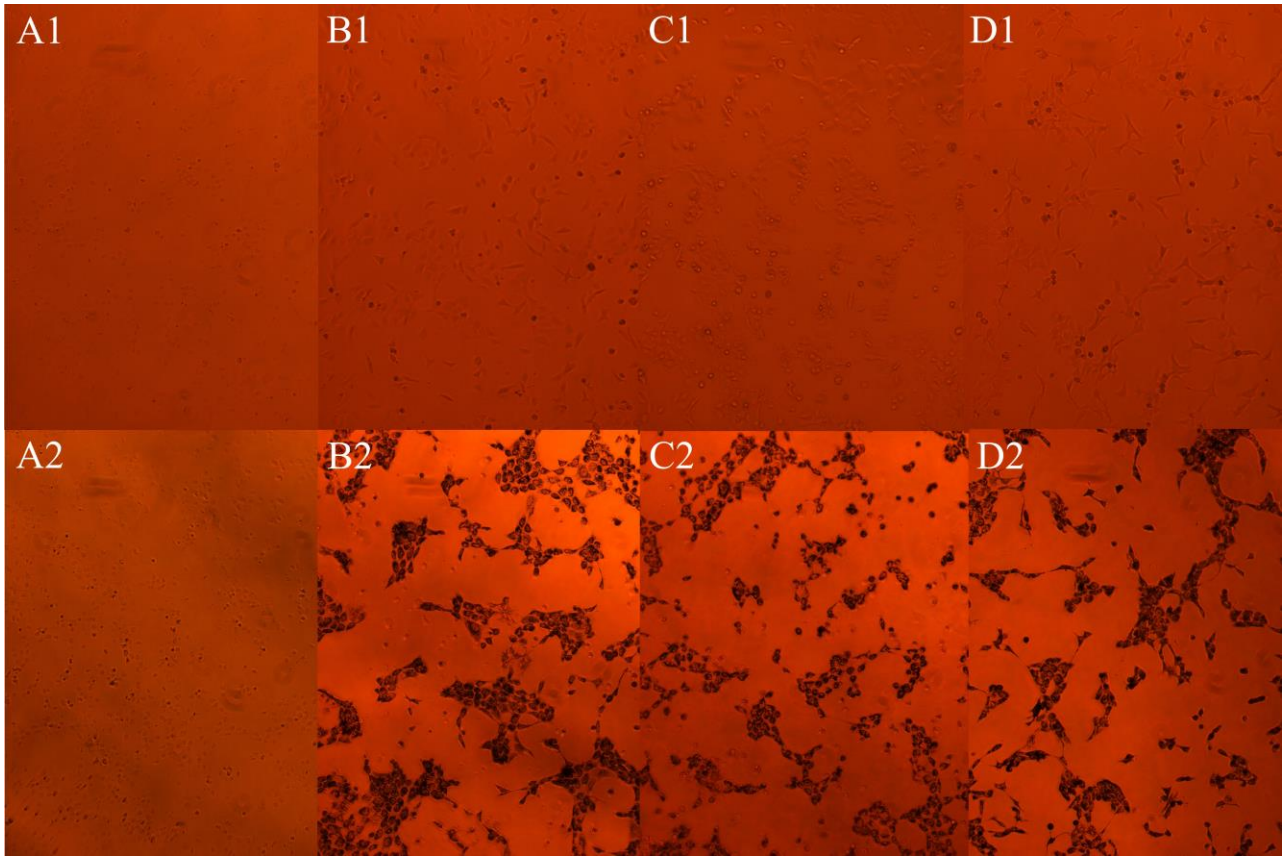

Figure 22: Micrograph of the third MTT experiment. Respectively A to D denotes triton, empty NPs, and NCE-containing NPs. The number 1 denotes before MTT addition, while 2 is after.

In summary; throughout experiments 1-3, the toxicity of NCE was assessed and the results were as following:

- NCE as a free drug in the range of 50-500 mg/mL was found to be non-toxic, and did not affect the cell viability.
- Encapsulated NCE in CL NPs in the range of 103.1 to 824.8 µg/mL were found to be non-toxic, and seem to increase cell viability.
- CL NPs were mostly found to be non-toxic as well not effecting cell viability.

5 Conclusions

In this project we assessed the cytotoxicity of NCE both as a free drug and encapsulated in CLNPs before potential *in vivo* testing can commence. Although our study suggested that NCE has no toxic effect on HaCaT cells further experiments should be carried out with longer incubation time to simulate real-time conditions of *in situ* exposure of the NCE-containing chitosan/lecithin nanoparticles. After optimization of the cell toxicity test further experiments can be performed on HaCaT cells, fibroblasts cell, and macrophages focusing on any potential hazards that may appear after the application of light irrigation with the intent of being a PDT candidate.

The optimization of chitosan/lecithin nanoparticles loaded with NCE needs to continue due to discrepancies between our study and the previous projects, as well as described in literature. Despite this, our entrapment efficiency seems to carry promise for future experimentations.

It is our belief that the HPLC method should be optimized with regards to detecting miniscule and less varying amounts of the NCE for more reliable and reproducible results.

6 Future perspectives

Short-term perspectives

- Optimization of NPs
    - Investigate the optimal amount of NCE to be entrapped
- Evaluation of NCE-mediated PDT against HaCaT cells, fibroblasts and macrophages.
- Optimization of empty CLNPs
- Optimization of MTT assay.
    - Assessment of NCE-containing NPs' incubation time.
    - Assessment of the empty CLNPs' incubation time.
- Optimization of HPLC method
    - Improve separation of the different products
    - Evaluate if an internal standard might improve the results in comparison to the NCE-solution used as a standard.

Long-term perspectives

- *In vivo* studies of the effect and safety of NCE.

7 References

1. Sen, C. K., G. M. Gordillo, S. Roy, R. Kirsner, L. Lambert, T. K. Hunt, F. Gottrup, G. C. Gurtner and M. T. Longaker (2009). "Human skin wounds: A major and snowballing threat to public health and the economy." Wound Repair and Regeneration **17**(6): 763-771.
2. Sherwood, L. (2012). Introduction to Human Physiology, Brooks/Cole.
3. Venus, M., J. Waterman and I. McNab (2010). "Basic physiology of the skin." Surgery (Oxford) **28**(10): 469-472.
4. Williams, A. (2003). Transdermal and Topical Drug Delivery from Theory to Clinical Practice, Pharmaceutical Press.
5. El Maghraby, G. M., B. W. Barry and A. C. Williams (2008). "Liposomes and skin: From drug delivery to model membranes." European Journal of Pharmaceutical Sciences **34**(4–5): 203-222.
6. Bouwstra, J. A. and M. Ponec (2006). "The skin barrier in healthy and diseased state." Biochimica et Biophysica Acta (BBA) - Biomembranes **1758**(12): 2080-2095.
7. Hwa, C., E. A. Bauer and D. E. Cohen (2011). "Skin biology." Dermatologic Therapy **24**(5): 464-470.
8. Hoffmann, J. N., A. G. Montag and N. J. Dominy (2004). "Meissner corpuscles and somatosensory acuity: The prehensile appendages of primates and elephants." The Anatomical Record Part A: Discoveries in Molecular, Cellular, and Evolutionary Biology **281A**(1): 1138-1147.
9. Cui, C.-Y. and D. Schlessinger (2015). "Eccrine sweat gland development and sweat secretion." Experimental Dermatology **24**(9): 644-650.
10. Benson, H. A. and A. C. Watkinson (2012). Transdermal and Topical Drug Delivery: Principles and Practice. Skin structure, function, and permeation, John Wiley & Sons Inc., NJ, USA**:** 3-22.
11. Otberg, N., H. Richter, H. Schaefer, U. Blume-Peytavi, W. Sterry and J. Lademann (2004). "Variations of Hair Follicle Size and Distribution in Different Body Sites." Journal of Investigative Dermatology **122**(1): 14-19.
12. Scharschmidt, T. C. and M. A. Fischbach (2013). "What lives on our skin: ecology, genomics and therapeutic opportunities of the skin microbiome." Drug Discovery Today: Disease Mechanisms **10**(3–4): e83-e89.
13. Sanford, J. A. and R. L. Gallo (2013). "Functions of the skin microbiota in health and disease." Seminars in Immunology **25**(5): 370-377.
14. Goering, R., H. Dockrell, M. Zuckerman, I. Roitt and P. L. Chiodini (2012). Mims' Medical Microbiology, Elsevier Health Sciences.
15. Lee, S. H., S. K. Jeong and S. K. Ahn (2006). "An update of the defensive barrier function of skin." Yonsei Medical Journal **47**(3): 293-306.
16. Lai-Cheong, J. E. and J. A. McGrath (2009). "Structure and function of skin, hair and nails." Medicine **37**(5): 223-226.
17. Hannigan, G. D. and E. A. Grice (2013). "Microbial Ecology of the Skin in the Era of Metagenomics and Molecular Microbiology." Cold Spring Harbor Perspectives in Medicine **3**(12): a015362.
18. Zeeuwen, P. L., M. Kleerebezem, H. M. Timmerman and J. Schalkwijk (2013). "Microbiome and skin diseases." Current Opinion in Allergy and Clinical Immunology **13**(5): 514-520.

19. Chen, Y. E. and H. Tsao (2013). "The skin microbiome: Current perspectives and future challenges." Journal of the American Academy of Dermatology **69**(1): 143-155.e143.
20. Broughton, G., 2nd, J. E. Janis and C. E. Attinger (2006). "The basic science of wound healing." Plastic and Reconstructive Surgery **117**(7 Suppl): 12s-34s.
21. Boateng, J. S., K. H. Matthews, H. N. E. Stevens and G. M. Eccleston (2008). "Wound Healing Dressings and Drug Delivery Systems: A Review." Journal of Pharmaceutical Sciences **97**(8): 2892-2923.
22. Velnar, T., T. Bailey and V. Smrkolj (2009). "The wound healing process: an overview of the cellular and molecular mechanisms." Journal of International Medical Research **37**(5): 1528-1542.
23. Strodtbeck, F. (2001). "Physiology of wound healing." Newborn and Infant Nursing Reviews **1**(1): 43-52.
24. Shaw, T. J. and P. Martin (2009). "Wound repair at a glance." Journal of Cell Science **122**(18): 3209-3213.
25. Gurtner, G. C., S. Werner, Y. Barrandon and M. T. Longaker (2008). "Wound repair and regeneration." Nature **453**(7193): 314-321.
26. Martin, J. M., J. M. Zenilman and G. S. Lazarus (2010). "Molecular Microbiology: New Dimensions for Cutaneous Biology and Wound Healing." Journal of Investigative Dermatology **130**(1): 38-48.
27. Singh, M. R., S. Saraf, A. Vyas, V. Jain and D. Singh (2013). "Innovative approaches in wound healing: trajectory and advances." Artificial Cells, Nanomedicine, and Biotechnology **41**(3): 202-212.
28. Davies, D. (2003). "Understanding biofilm resistance to antibacterial agents." Nature Reviews Drug Discovery **2**(2): 114-122.
29. James, G. A., E. Swogger, R. Wolcott, E. d. Pulcini, P. Secor, J. Sestrich, J. W. Costerton and P. S. Stewart (2008). "Biofilms in chronic wounds." Wound Repair and Regeneration **16**(1): 37-44.
30. O'Toole, G., H. B. Kaplan and R. Kolter (2000). "Biofilm Formation as Microbial Development." Annual Review of Microbiology **54**(1): 49-79.
31. Percival, S. L., S. M. McCarty and B. Lipsky (2015). "Biofilms and Wounds: An Overview of the Evidence." Advances in Wound Care **4**(7): 373-381.
32. Taraszkiewicz, A., G. Fila, M. Grinholc and J. Nakonieczna (2013). "Innovative Strategies to Overcome Biofilm Resistance." BioMed Research International **2013**: 13.
33. Demidova-Rice, T. N., M. R. Hamblin and I. M. Herman (2012). "Acute and impaired wound healing: pathophysiology and current methods for drug delivery, part 1: normal and chronic wounds: biology, causes, and approaches to care." Advances in Skin & Wound Care **25**(7): 304-314.
34. Vogeleer, P., Y. D. N. Tremblay, A. A. Mafu, M. Jacques and J. Harel (2014). "Life on the outside: role of biofilms in environmental persistence of Shiga-toxin producing Escherichia coli." Frontiers in Microbiology **5**: 317.
35. Cieplik, F., L. Tabenski, W. Buchalla and T. Maisch (2014). "Antimicrobial photodynamic therapy for inactivation of biofilms formed by oral key pathogens." Frontiers in Microbiology **5**: 405.
36. Bechet, D., P. Couleaud, C. Frochot, M.-L. Viriot, F. Guillemin and M. Barberi-Heyob (2008). "Nanoparticles as vehicles for delivery of photodynamic therapy agents." Trends in Biotechnology **26**(11): 612-621.
37. Allison, R. R., G. H. Downie, R. Cuenca, X.-H. Hu, C. J. H. Childs and C. H. Sibata (2004). "Photosensitizers in clinical PDT." Photodiagnosis and Photodynamic Therapy **1**(1): 27-42.

38. Valenta, C., B. G. Auner and I. Loibl (2005). "Skin permeation and stability studies of 5-aminolevulinic acid in a new gel and patch preparation." Journal of Controlled Release **107**(3): 495-501.
39. Wachowska, M., A. Muchowicz, M. Firczuk, M. Gabrysiak, M. Winiarska, M. Wańczyk, K. Bojarczuk and J. Golab (2011). "Aminolevulinic Acid (ALA) as a Prodrug in Photodynamic Therapy of Cancer." Molecules **16**(5): 4140.
40. Fotinos, N., M. A. Campo, F. Popowycz, R. Gurny and N. Lange (2006). "5-Aminolevulinic Acid Derivatives in Photomedicine: Characteristics, Application and Perspectives." Photochemistry and Photobiology **82**(4): 994-1015.
41. Hadafow, M. A. (2014). Chitosan-based Drug Delivery Dystem for a New Chemical Entity
for Photodynamic Wound Therapy. Masters Masters, The University of Tromsø The Arctic University of Norway.
42. Hemmingsen, L. M. (2015). Chitosan Lecithin Nanoparticles with New Chemical: Entity Antimicrobial Evaluation. Masters Masters, The University of Tromsø The Arctic University of Norway.
43. Thoresen, I. E. (2014). Advanced Drug Delivery System for New Chemical Entity Destined for Wound Therapy: Anti-biofilm Potential of Novel Drug Delivery System. Masters Masters, University of Tromsø The Arctic University of Norway.
44. Buzea, C., I. I. Pacheco and K. Robbie (2007). "Nanomaterials and nanoparticles: Sources and toxicity." Biointerphases **2**(4): MR17-MR71.
45. Oberdörster, G., V. Stone and K. Donaldson (2007). "Toxicology of nanoparticles: A historical perspective." Nanotoxicology **1**(1): 2-25.
46. Webster, T. J. (2007). "IJN's second year is now a part of nanomedicine history!" International Journal of Nanomedicine **2**(1): 1-2.
47. Cornelia, M. W., M. Amandine, N. Thomas, V. François, L. Fabrice and J. Marie-Odile (2015). "The Ins and Outs of Nanoparticle Technology in Neurodegenerative Diseases and Cancer." Current Drug Metabolism **16**(8): 609-632.
48. Mohanraj, V. and Y. Chen (2007). "Nanoparticles-a review." Tropical Journal of Pharmaceutical Research **5**(1): 561-573.
49. Sonvico, F., A. Cagnani, A. Rossi, S. Motta, M. T. Di Bari, F. Cavatorta, M. J. Alonso, A. Deriu and P. Colombo (2006). "Formation of self-organized nanoparticles by lecithin/chitosan ionic interaction." International Journal of Pharmaceutics **324**(1): 67-73.
50. Pal, S. L., U. Jana, P. Manna, G. Mohanta and R. Manavalan (2011). "Nanoparticle: an overview of preparation and characterization." Journal of Applied Pharmaceutical Science **1**(6): 228-234.
51. Maghraby, G. M. M. E., A. C. Williams and B. W. Barry (2006). "Can drug-bearing liposomes penetrate intact skin?" Journal of Pharmacy and Pharmacology **58**(4): 415-429.
52. Hurler, J., O. A. Berg, M. Skar, A. H. Conradi, P. J. Johnsen and N. Škalko-Basnet (2012). "Improved Burns Therapy: Liposomes-in-Hydrogel Delivery System for Mupirocin." Journal of Pharmaceutical Sciences **101**(10): 3906-3915.
53. Uchechi, O., J. D. Ogbonna and A. A. Attama (2014). Nanoparticles for dermal and transdermal drug delivery, InTech.
54. Prow, T. W., J. E. Grice, L. L. Lin, R. Faye, M. Butler, W. Becker, E. M. T. Wurm, C. Yoong, T. A. Robertson, H. P. Soyer and M. S. Roberts (2011). "Nanoparticles and microparticles for skin drug delivery." Advanced Drug Delivery Reviews **63**(6): 470-491.
55. Kimura, E., Y. Kawano, H. Todo, Y. Ikarashi and K. Sugibayashi (2012). "Measurement of Skin Permeation/Penetration of Nanoparticles for Their Safety Evaluation." Biological and Pharmaceutical Bulletin **35**(9): 1476-1486.

56. Witting, M., K. Obst, W. Friess and S. Hedtrich (2015). "Recent advances in topical delivery of proteins and peptides mediated by soft matter nanocarriers." Biotechnology Advances **33**(6, Part 3): 1355-1369.
57. Pelgrift, R. Y. and A. J. Friedman (2013). "Nanotechnology as a therapeutic tool to combat microbial resistance." Advanced Drug Delivery Reviews **65**(13–14): 1803-1815.
58. Zhang, J., W. Xia, P. Liu, Q. Cheng, T. Tahirou, W. Gu and B. Li (2010). "Chitosan Modification and Pharmaceutical/Biomedical Applications." Marine Drugs **8**(7): 1962-1987.
59. Jayakumar, R., D. Menon, K. Manzoor, S. V. Nair and H. Tamura (2010). "Biomedical applications of chitin and chitosan based nanomaterials—A short review." Carbohydrate Polymers **82**(2): 227-232.
60. Ravi Kumar, M. N. V. (2000). "A review of chitin and chitosan applications." Reactive and Functional Polymers **46**(1): 1-27.
61. Baldrick, P. (2010). "The safety of chitosan as a pharmaceutical excipient." Regulatory Toxicology and Pharmacology **56**(3): 290-299.
62. Dash, M., F. Chiellini, R. M. Ottenbrite and E. Chiellini (2011). "Chitosan—A versatile semi-synthetic polymer in biomedical applications." Progress in Polymer Science **36**(8): 981-1014.
63. Seyfarth, F., S. Schliemann, P. Elsner and U. C. Hipler (2008). "Antifungal effect of high- and low-molecular-weight chitosan hydrochloride, carboxymethyl chitosan, chitosan oligosaccharide and N-acetyl-d-glucosamine against Candida albicans, Candida krusei and Candida glabrata." International Journal of Pharmaceutics **353**(1–2): 139-148.
64. Croisier, F. and C. Jérôme (2013). "Chitosan-based biomaterials for tissue engineering." European Polymer Journal **49**(4): 780-792.
65. Xu, Q., M. Nakajima, T. Shiina and Z. Liu (2011). Soybean-based Surfactants and Their Applications, INTECH Open Access Publisher.
66. Hafner, A., M. Durrigl, I. Pepic and J. Filipovic-Grcic (2011). "Short- and long-term stability of lyophilised melatonin-loaded lecithin/chitosan nanoparticles." Chemical and Pharmaceutical Bulletin (Tokyo) **59**(9): 1117-1123.
67. Shah, H. and K. Singh. (2015, 2015.10.02). "Lecithin." from https://www.medicinescomplete.com/mc/excipients/2012/1001940783.htm.
68. El-Ansary, A. and S. Al-Daihan (2009). "On the Toxicity of Therapeutically Used Nanoparticles: An Overview." Journal of Toxicology **2009**: 9.
69. Arora, S., J. M. Rajwade and K. M. Paknikar (2012). "Nanotoxicology and in vitro studies: The need of the hour." Toxicology and Applied Pharmacology **258**(2): 151-165.
70. Schaeublin, N. M., L. K. Braydich-Stolle, A. M. Schrand, J. M. Miller, J. Hutchison, J. J. Schlager and S. M. Hussain (2011). "Surface charge of gold nanoparticles mediates mechanism of toxicity." Nanoscale **3**(2): 410-420.
71. Andón, F. T. and B. Fadeel (2014). Nanotoxicology: Towards Safety by Design. Nano-Oncologicals: New Targeting and Delivery Approaches. J. M. Alonso and M. Garcia-Fuentes. Cham, Springer International Publishing**:** 391-424.
72. Huang, Y.-W., C.-h. Wu and R. S. Aronstam (2010). "Toxicity of Transition Metal Oxide Nanoparticles: Recent Insights from in vitro Studies." Materials **3**(10): 4842.
73. Takhar, P. and S. Mahant (2011). "In vitro methods for nanotoxicity assessment: advantages and applications." Archives of Applied Science Research **3**(2): 389-403.
74. Mosmann, T. (1983). "Rapid colorimetric assay for cellular growth and survival: Application to proliferation and cytotoxicity assays." Journal of Immunological Methods **65**(1): 55-63.
75. Sittampalam, G., N. Gal-Edd and M. Arkin (2004). Assay Guidance Manual [Internet], Eli Lilly & Company/National Center for Advancing Translational Sciences.

76. Berridge, M. V. and A. S. Tan (1993). "Characterization of the Cellular Reduction of 3-(4,5-dimethylthiazol-2-yl)-2,5-diphenyltetrazolium bromide (MTT): Subcellular Localization, Substrate Dependence, and Involvement of Mitochondrial Electron Transport in MTT Reduction." Archives of Biochemistry and Biophysics **303**(2): 474-482.
77. Borenfreund, E., H. Babich and N. Martin-Alguacil (1988). "Comparisons of two in vitro cytotoxicity assays—The neutral red (NR) and tetrazolium MTT tests." Toxicology in Vitro **2**(1): 1-6.
78. Denizot, F. and R. Lang (1986). "Rapid colorimetric assay for cell growth and survival." Journal of Immunological Methods **89**(2): 271-277.
79. Andersen, T., Ž. Vanić, G. E. Flaten, S. Mattsson, I. Tho and N. Škalko-Basnet (2013). "Pectosomes and Chitosomes as Delivery Systems for Metronidazole: The One-Pot Preparation Method." Pharmaceutics **5**(3): 445-456.
80. Frantzen, C. B., L. Ingebrigtsen, M. Skar and M. Brandl (2003). "Assessing the accuracy of routine photon correlation spectroscopy analysis of heterogeneous size distributions." American Association of Pharmaceutical Scientists **4**(3): 62-70.
81. Şenyiğit, T., F. Sonvico, S. Barbieri, Ö. Özer, P. Santi and P. Colombo (2010). "Lecithin/chitosan nanoparticles of clobetasol-17-propionate capable of accumulation in pig skin." Journal of Controlled Release **142**(3): 368-373.
82. Tan, Q., W. Liu, C. Guo and G. Zhai (2011). "Preparation and evaluation of quercetin-loaded lecithin-chitosan nanoparticles for topical delivery." International Journal of Nanomedicine **6**: 1621-1630.
83. Özcan, I., E. Azizoglu, T. Senyigit, M. Ozyazici and O. Ozer (2013). "Comparison of PLGA and lecithin/chitosan nanoparticles for dermal targeting of betamethasone valerate." Journal of Drug Targeting **21**(6): 542-550.
84. Hafner, A., J. Lovric, I. Pepic and J. Filipovic-Grcic (2011). "Lecithin/chitosan nanoparticles for transdermal delivery of melatonin." Journal of Microencapsulation **28**(8): 807-815.
85. Clogston, J. D. and A. K. Patri (2011). Zeta Potential Measurement. Characterization of Nanoparticles Intended for Drug Delivery. E. S. McNeil. Totowa, NJ, Humana Press**:** 63-70.
86. Harris, F. and L. Pierpoint (2012). "Photodynamic therapy based on 5-aminolevulinic acid and its use as an antimicrobial Agent." Medicinal Research Reviews **32**(6): 1292-1327.
87. Elnaggar, Y. S. R., W. M. El-Refaie, M. A. El-Massik and O. Y. Abdallah (2014). "Lecithin-based nanostructured gels for skin delivery: An update on state of art and recent applications." Journal of Controlled Release **180**: 10-24.
88. Paolino, D., C. A. Ventura, S. Nisticò, G. Puglisi and M. Fresta (2002). "Lecithin microemulsions for the topical administration of ketoprofen: percutaneous adsorption through human skin and in vivo human skin tolerability." International Journal of Pharmaceutics **244**(1–2): 21-31.
89. Lai, L.-h., Q.-h. Fu, Y. Liu, K. Jiang, Q.-m. Guo, Q.-y. Chen, B. Yan, Q.-q. Wang and J.-g. Shen (2012). "Piperine suppresses tumor growth and metastasis in vitro and in vivo in a 4T1 murine breast cancer model." Acta Pharmacologica Sinica **33**(4): 523-530.
90. Loh, J. W., M. Saunders and L.-Y. Lim (2012). "Cytotoxicity of monodispersed chitosan nanoparticles against the Caco-2 cells." Toxicology and Applied Pharmacology **262**(3): 273-282.